Fermi National Accelerator Laboratory

FN-454
7000.660

Phenomenological Summary of Dechanneling in Aligned Single Crystals

R.A. Carrigan, Jr.
Fermi National Accelerator Laboratory
P.O. Box 500, Batavia, Illinois 60510

May 1987

Operated by Universities Research Association Inc. under contract with the United States Department of Energy

PHENOMENOLOGICAL SUMMARY OF DECHANNELING IN ALIGNED SINGLE CRYSTALS

Richard A. Carrigan, Jr.

Fermi National Accelerator Laboratory

Batavia, Illinois 60510

ABSTRACT

The current status of particle dechanneling in single crystals is reviewed. The theoretical situation for dechanneling is considered for the conventional case, for bending, and for imperfections. The experimental results from both the MeV and the GeV regime are summarized. Defect dechanneling limitations are surveyed for high energy channeling. Lepton and heavy negative particle dechanneling are also discussed. Finally, the dechanneling information needed for the future is summarized.

I. Introduction

Positively charged particles moving in channels in aligned single crystals are adiabatically scattered out of the channels or dechanneled. This fact represents a major limitation for the practical application of channeling to several processes. On the other hand, this feature has also been used as a powerful tool to study material structures such as defects[1].

The principal dechanneling mechanism for positive particles is a combination of electronic multiple scattering when the particles are moving near the center of the channel along with multiple scattering off the vibrating nuclei of the atoms in the atomic strings as the dechanneling particles near the edge of the channel. For planar channeling the first process is dominant. For axial channeling both processes contribute and the presence of lattice vibrations leads to the possibility of a significant temperature-sensitive effect.

The picture for negatively charged particles is somewhat different since they move near the nuclear centers in the atomic strings or planes when they are channeled. As a result, the nuclear multiple scattering is always the

dominant part. So far there has been little analytic treatment of negative dechanneling although there have been Monte Carlo studies[2].

This combination of multiple scattering processes in particle dechanneling is a complicated problem in diffusion requiring sophisticated mathematical techniques for a fundamental treatment[3,4]. In addition to this diffusion process in a perfect crystal lattice one must also consider the effects of scattering by point interstitial defects and the possibility of abrupt discontinuities due to dislocations.

A perfect theory of dechanneling would then have to explain a number of features. It would have to give the relation of planar to axial channeling so that one could extrapolate measurements in one case to the other. In particular it would have to provide a recipe for interpolating temperature-dependent effects in the case of axial channeling. In the same sense it would have to explain the relation of dechanneling for different planes and axes of a crystal as well as the interrelationship between different crystals. An important characteristic of the dechanneling mechanism is its functional dependence on the particle energy. Basically the dechanneling length goes as 1/E. This relation must be properly treated over a range of energies from non-relativistic to ultra-relativistic.

At nuclear physics energies (the MeV range) beams of particles used for channeling usually have an angular spread somewhat smaller than the critical angle (a so-called "pencil" beam). For GeV energies the beam divergence tends to be much larger than the critical angle. The pencil beam is easier to treat in a diffusion picture. The other case requires an integration over the angular phase space of the incident beam.

The perfect theory should also give the relationship between negative and positive dechanneling as well as that between heavy particles and electrons and positrons. The effects of defects, such as dislocations and interstitials, should be easily incorporated. Again the functional energy dependence for different defect types should be predicted. It is also desirable that such models be cast in terms of actual measures of defect concentration, such as those given by x-ray double scattering studies.

The theory should gracefully interpolate to the bent crystal case so that it gives "normal" dechanneling for that situation. The channeling acceptance should be predicted for a uniformly curved crystal as well as one with continuously changing curvature. It should also treat exotic substances such as strain-layer super lattices[5], one and two dimensional

conductors[6], poly-crystaline materials such as highly oriented pyrolytic graphite[7], and even materials such as zeolite structures[8].

Suffice it to say that a perfect, all-encompassing theory is not available. Seeking such a theory is a wonderful goal. However more modest efforts are also important. For example, a full axial-planar diffusion model with an accompanying analytical phenomenology to scale to different crystals and geometries would be very useful.

Why is dechanneling information important? The utility of such information in solid state science has been established by more than a decade of intense work[1]. In particle physics and accelerator science several speculative applications of channeling have been proposed. Indeed, bent crystals have already been used at Fermilab as beam elements in two practical high energy particle beams[9]. More information is needed, particularly for germanium and tungsten, to further such applications. P. Chen and R. J. Noble[10] have recently looked in detail at the possibility of solid state accelerators where channeling and dechanneling could be important factors. While realizations of these concepts are admittedly very far from application, the studies point out the importance of better understanding of dechanneling in exotic materials.

This article reviews dechanneling with a particular emphasis on experimental channeling at high energy. It is not meant to be a serious discussion of the theory of dechanneling or defect dechanneling.

In the following sections a number of aspects of dechanneling will be considered. Section II covers the theory of ordinary dechanneling, Section III-dechanneling due to imperfections, and Section IV-the theory of bending dechanneling. Section V discusses measurements of ordinary dechanneling, Section VI-bending dechanneling, and Section VII-defect dechanneling. Section VIII considers the interesting subjects of positrons, electrons, and heavy negative particles. Finally Section IX summarizes dechanneling information needed for the future.

II. Theory of Ordinary Dechanneling

Ordinary dechanneling is simply multiple scattering of particles out of a channel. A useful approach is to compare the channeling critical angle to the rate of multiple scattering. This picture was originally formulated by Lindhard[3] and also used by Feldman et al.[11] for planar channeling. In this picture the dechanneling length is approximately equal to the square of the channeling angle divided by the rate of change with distance of the mean square angle of multiple scattering. For planar channeling the electronic multiple scattering angle is appropriate. The planar dechanneling length (1/e) is then:

$$\lambda = 1.62\ \psi^2_{cp}/\langle\theta^2\rangle_c \qquad (1)$$

Here ψ_{cp} is the planar critical angle and $\langle\theta^2\rangle_c$ is some approximation to the average of the square of the multiple scattering in the channel. This form of the expression is interesting because it immediately gives the energy dependence. Of course care must be taken to express both the critical angle and the multiple scattering angle in their

correct relativistic forms and to use angles that correspond to the same points on the statistical distributions.

Evaluation of the multiple scattering angle requires the determination of the minimum (b_{min}) and maximum (b_{max}) impact parameters for the collisions of the beam particles (typically pions or protons) with the electrons in the channel. These impact parameters enter in logarithmic terms to give some logarithmic energy dependence. However both parameters saturate. b_{max} can be no larger than the half width of the channel. b_{min} can be no smaller than the size of the beam particle, on the order of a Fermi. As a result, these logarithmic terms lead to no significant energy dependence above 1 MeV.

In this picture $\langle\theta^2\rangle_c$ is inversely proportional to the radiation length in the channel. The problem is how this is evaluated and for what part of the channel. The point-of-view that follows corresponds more closely to the uniform illumination of the channel that occurs in multi-GeV beams than to the "pencil" beams of MeV experiments.

The ratio of the average electronic radiation length to the conventional case is approximately equal to $2Z^*L_{n0}/L_{e0}$ where Z^* is the effective electron number in the channel. In what follows Z^* has been set equal to Z, although it is easy

to argue that it might be less for planar channeling. L_{n0} and L_{e0} are the logarithmic terms for energy loss on nuclei and electrons respectively. (See, for example, Gemmell[12], but note that this is not correct for relativistic energies.) L_{n0} and L_{e0} must be evaluated at points where the energy dependence on b_{min} and b_{max} has saturated (several Mev). For the evaluation that follows the ratio of L_{n0}/L_{e0} has been set equal to 2.

For this situation

$$\lambda = 1.095*10^{-3}nZZ^{*}ap\beta L_{NR}(L_{n0}/L_{e0})F_{PS} \qquad (2)$$

where n is the areal density in Angstroms^{-2}, Z is the atomic number, a is the Thomas-Fermi screening distance in Angstroms, p is the momentum in GeV/c, β is the ratio of the velocity to the speed of light, L_{NR} is the normal radiation length, and F_{PS} is defined in Gemmell[12].

At 100 GeV this gives λ = 5.5 cm for Si(110). In Section V a fit to both the MeV and GeV data is found to give 7.0 cm as the dechanneling length at 100 GeV (for uniform illumination of the channel). In view of all the approximations and experimental uncertainties this is remarkably close. For 5 MeV channeling, Feldman et al.[11] obtained 2.5 microns from a similar calculation and found an experimental number of 9.0

microns. (Both numbers are half lengths.) Here the experimental number should be somewhat larger since one is dealing with a pencil beam. This formula also reproduces the relationship of the dechanneling length for different planar orientations in the same material. The relationship between silicon and germanium is also correct to within the experimental error. The phenomenological length for tungsten is longer than the fit given in Table V based on the early experimental work of Davies et al.[13]. Note however, that later work by the same group[14] seems to give longer dechanneling lengths. While both the numbers from the GeV and the MeV regimes are the right orders of magnitude, it must be emphasized that this phenomenological fit is an approximate picture.

A more complete treatment requires the solution of the diffusion equation related to multiple scattering[15]. For the axial case this is:

$$\frac{\partial g(E_T,z)}{\partial z} = \frac{\partial}{\partial E_T} A(E_T)\ D(E_T) \frac{\partial}{\partial E_T} \frac{g(E_T,z)}{A(E_T)} \qquad (3)$$

By assuming statistical equilibrium over an accessible area one reduces a four dimensional problem to a one dimensional case. Here $g(E_T,z)$ is the distribution of particles in

transverse energy at some depth z into the crystal, $A(E_T)$ is the area accessible to a particle at some transverse energy E_T, and $D(E_T)$ is the diffusion function for the process. The transverse energy is the energy of a particle in an equivalent crystal potential. A more felicitous but less phenomenological formulation was given originally by Lindhard[3]. He expresses the equation in terms of transverse momentum.

The key to this equation is the diffusion function. For an amorphous crystal this would correspond to a conventional solution of the multiple scattering problem. For a crystal the diffusion function must reflect the varying charge density across the channel. This charge density must factor in both electrons and nuclei and also include the effect of lattice vibrations. Bonderup at al.[4,15] have treated this problem for axial channeling in some detail. They find reasonable agreement for MeV energies in silicon and tungsten. Campisano et al.[16] have examined this for both axial and planar cases in the MeV region for Si and Ge using a so-called steady increase model in which the diffusion coefficient is assumed to increase linearly with transverse energy. They also find agreement. They claim a functional dependence for the dechanneling fraction that goes as the square of the lattice vibrations. On the other hand the experiments of Davies et al.[14] on tungsten do not support this scaling. Matsunami and Howe[17] have reviewed this and

conclude "...Except for a very limited region at quite low z/E values (<1micron/MeV) neither the theoretical calculations or the experimental data suggest a simple scaling of the dechanneling fraction with z/E."

A problem with some diffusion models such as Bonderup et al.[4,15] is that the diffusion function must be calculated numerically. Matsunami and Howe[17] have suggested that an analytic form is useful for investigating temperature and energy dependence for different projectiles and for understanding dechanneling by defects. They have devised analytical forms for the axial case. These forms seem to give good agreement for Si and Ge in the 1.0 to 1.6 MeV range.

Ohtsuki and his collaborators[18] have undertaken a study of the diffusion function from first principals. They argue that the problem of incorporating lattice vibrations must be approached using quantum mechanics. Otherwise the calculation is correct over only a small regime of energy and transverse energy. They state that the original Lindhard calculation corresponds only to single phonon excitations. This would be equivalent to hyperchanneling at very low energy. Ohtsuki also takes note of Ellegard and Lassens' recognition[19] that the Gaussian type diffusion coefficient is more reasonable than the Lindhard type. Ohtsuki and collaborators[20] evaluate the diffusion coefficient using an inelastic scattering

function. An important facet of this approach is the treatment using plasmons in a nearly free electron gas. Ohtsuki's diffusion functions tend to be somewhat smaller than the Lindhard form in the center of the channel. At the edge the two are closer to agreement. This is illustrated in Figure 1 and Figure 2. Figure 2 shows both the electronic and nuclear parts.

Ohtsuki has also extended the treatment to slow ions in the electron gas by making use of a Green's function technique. In this way he is able to fit the energy dependence down to 0.5 MeV.

Ohtsuki's student, H. Nitta, has recently completed a very thorough study of this fundamental treatment of the diffusion function[22]. He has broadened the approach to give consistency between the kinetic equation and the definition of the local diffusion coefficient.

In point of fact the diffusion equation is an approximation to a more general situation. The diffusion equation assumes scatterings are small. Instead one can start with the Chapman-Kolmogorov equation used for Markov processes and make certain expansions that give rise to the Fokker-Planck equation. Alternatively a differential approach can be taken. This is through the master equation. The master equation

gives the probability distribution at a distance z+dz if it is known at z. However the master equation is more complicated to solve than the diffusion equation. In the Bonderup et al.[4,15] treatment of axial channeling they essentially start with the Chapman-Kolmogorov equation, go to the master equation, and then approximate with the diffusion equation.

Typically these more sophisticated approaches are used to try to overcome a limitation of the diffusion equation. For example, Kumakhov and Wedell[23] have used the Fokker-Planck equation in phase space to avoid the requirement of statistical equilibrium. Gärtner and collaborators[24-28] employ the master equation to study defect dechanneling where the small scattering approximation may no longer be appropriate and where the effects of energy loss can be significant.

Sometimes a stochastic equation is used for the diffusion problem[29]. The stochastic equation is similar to the master equation. When the stochastic equation is expanded in series and the first two terms are retained a Fokker-Planck equation is obtained. Belotshitsky et al.[30] have shown that this reduces to a diffusion equation under certain circumstances. However Oshiyama and Mannami[29] argue that this is not always a good approximation. This would appear to be particularly true near the edge of a channel. They suggest that this effect is not negligible for axial channeling.

Many of these calculations assume a beam with an angular divergence much less than the critical angle. For planar channeling at high energy the situation is usually reversed. Vorobiev and collaborators have examined the impact of this possibility[31]. They assume that the valence electrons are uniformly distributed and are the only ones that contribute to the dechanneling. Their results are illustrated in Figure 3. While this approach is open to criticism, it does illustrate how the dechanneling length decreases as the beam angular divergence increases.

In his review of channeling in the early seventies, Gemmell[12] made some succinct observations on the problems of theoretical dechanneling estimates. Many of his points are as true now as they were then. They include:

1. "The calculated contribution of electronic multiple scattering is sensitively dependent upon the expression used for the electron-density distribution. Expressions used thus far are probably not very accurate at large distances."

2. "Planar effects are ignored in most calculations on axial dechanneling. However experiments indicate that the feeding of particles from axial into planar channels

is an important dechanneling mechanism."

3. "The calculated dechanneling is sensitive to the choice of the critical transverse energy. Various choices have been made. Some of these have included temperature-dependent effects; others have not."

4. "The implied assumption that the rms thermal vibration amplitude is small compared to the distance of the channeled particles from the rows can be seriously in error for particles with high transverse energy.".

5. "In most theoretical treatments, it is usually assumed that rechanneling can be neglected. That is, the probability for transitions from the random beam into the aligned beam is assumed to be small."

III. Dechanneling Due to Imperfections

Defects in crystals produce significant and important effects on channeling. These are never for the better. A modern theoretical treatment of these processes which also includes normal dechanneling has been given by Gärtner and his colleagues[24-28].

Feldman, Mayer, and Picraux (FMP)[1] have provided a useful summary of dechanneling due to imperfections. They give as the probability of dechanneling per unit length

$$\frac{dP_D}{dz} = \sigma_D n_D(z) \qquad (4)$$

Here σ_D is the dechanneling factor (see Table I) and n_d is the defect density. For point defects σ_D corresponds to a cross section. From an application point these defects divide into three classes; interstitials, dislocations, and stacking faults.

An interstitial nucleus in a channel gives rise to much larger deflections than the electron cloud in the channel. FMP[1] give an estimate of the dechanneling factor as

$$\sigma_D \approx \frac{\pi}{2} \frac{Z_1 Z_2 e^2 d}{E} = 2.3 \times 10^{-21} \frac{Z_1 Z_2 d}{E} \text{ cm}^2 \qquad (5)$$

Here Z_1 and Z_2 are the atomic numbers of the beam particles and the crystal atoms respectively, d is the atomic spacing along an axis, and E is the kinetic energy for the non-relativistic case. In the second part of the formula d is in Angstroms and E is in MeV. As an example, σ_D=1.7*10^{-19} cm^2 for 2 MeV He ions along the <100> axis of Si where d=5.43 A. Note that the dechanneling per unit length is inversely proportional to the energy so that the impact of interstitial defects is correspondingly lower at high energy.

Dislocations extending transverse to the direction of particle motion correspond to line defects so that they have an equivalently larger "cross section". The dechanneling due to dislocations was first treated by Quere[32]. For dislocations the dechanneling factor can be approximated by

$$\sigma_D = \frac{b}{\pi \psi_{1/2}} \qquad (6)$$

where b is the Burger's vector representing the magnitude of the dislocation and $\psi_{1/2}$ is the half angle corresponding to the critical angle. Notice that since the critical angle is

inversely proportional to $\sqrt{E}$ that the probability of dechanneling per unit length will be proportional to the square root of the energy. Note, however, that for dislocation loops with small radii of curvature this energy dependence will eventually saturate.

The dislocation density varies widely for different materials. It ranges from approximately zero for the silicon used in the high energy channeling experiments to $10^{11}/cm^2$ in some cold-worked metals. The experimentally-measured dechanneling probability for silicon containing a fairly high dislocation density is illustrated in Figure 4 (from FMP[1]) for both axial and planar channeling in the MeV range. Notice that the experimental data do confirm the theoretical form.

A more rigorous treatment includes the flux distribution of the channeled particles. This type of calculation has been carried out by a number of authors including Ellison and Picraux[34], Kudo[35,36], Wielunski et al.[37,38], and Zakowicz and Pantell[39]. Interestingly, this type of theoretical formulation has since been used to study dechanneling in bent crystals.

Two other volume defects, stacking faults and twins, also lead to dechanneling. The dechanneling probability for these is only weakly dependent on energy.

Figure 5 from FMP[1] schematically illustrates the behavior with energy of the three major defect types. Which of the defects limits channeling in a crystal is a sensitive function of the defect density. Clearly the impact of dislocations ultimately becomes much more significant at very high energy.

Defect channeling touches on another subject, channeling behavior in exotic materials such as strained-layer superlattices[5], one and two dimensional conductors[6], and polycrystaline material such as highly-oriented pyrolytic graphite(HOPG)[7]. The dechanneling behavior of some of these exotics is intimately related to the possibility of using the channeling process in solid state accelerators[10]. But note that even very good, commercially-available HOPG has a mosaic spread of 0.2 degrees. The strained-layer superlattice is an interesting case in its own right. It is possible to produce resonance dechanneling by choosing the layer spacing to be comparable to the wavelengths of the channeling oscillations[5,40].

IV. Theory of Bending Dechanneling

The first serious suggestion that channeling in bent crystals could be used to deflect charged particles was made by E. Tsyganov[41] in 1976. The process has since been studied extensively in experiments at Dubna[42], Fermilab[43-45], and CERN[46]. Some work has also been done at Gatchina[47] at the relatively "low" energy of 1.0 GeV.

The basic bending process is almost obvious for a curved planar geometry. A positive particle inside the critical angle of a planar channel will follow the curved planes provided the curvature of the crystal is not too large. Dechanneling still occurs, due to both ordinary dechanneling, as well as certain features of the bending process. The actual potential well in the channel is modified by a linear centrifugal potential barrier that depends on the local crystal curvature. Figure 6, from Kudo[48], shows how this occurs. For a relativistic particle and a small enough bending radius (the Tsyganov radius)

$$R_T = E/eE_C \quad , \qquad (7)$$

the centrifugal barrier exactly equals the depth of the normal (no bending) potential and particles are no longer

deflected. Here E is the total energy of the particle and E_c is the interatomic field intensity at a distance from the plane of the crystal lattice where the trajectory of the particle no longer remains stable due to its interactions with individual atoms. In practice, the process is no longer practically useful well before the Tsyganov radius is reached.

For a bent crystal, the oscillatory trajectories shift toward one of the atomic planes, with the center of their oscillation given by the equilibrium position determined by the bottom of the modified potential well as shown in Figure 6. This shifted trajectory is shown in Figure 7b. It is easy to see that particles with amplitudes of oscillation greater than x_c will be dechanneled. As the crystal curvature increases from zero, particles with oscillation amplitudes near the critical value will begin to approach the plane almost immediately and thus be dechanneled.

It is useful to describe particle motion and the effects of bending in terms of a phase space composed of the transverse position coordinate for the particle relative to the center line of the plane and the angle of the particle relative to the planar direction. This is illustrated in Figure 8. Particles within the open ovals will continue to be channeled in the bent crystal, whereas those within the

hatched region will follow a path such as that indicated by the dashed trajectory shown. Such particles will approach the plane with amplitude larger than x_c, and hence be dechanneled. Calculation of the fraction of channeled particles that dechannel because of this centrifugal shift of the equilibrium point of their trajectory can be carried out if the form of the planar potential is known and if the critical distance of approach, x_c, is given. Such calculations have been made for a harmonic potential by Ellison and Picraux[34] and for more realistic Thomas-Fermi type potentials by Ellison[49] and by Kudo[48].

Ellison's results for particles dechanneled upon entering a region of constant curvature are shown in Figure 9. This calculation uses a Moliere approximation to the Thomas-Fermi potential. It makes use of the following assumptions: (1) the channeled particles have a statistical equilibrium distribution of trajectories when they reach the bend; (2) a particle is dechanneled if it penetrates too close ($x>x_c$) to a plane at any point of its trajectory; (3) the bent planes can be modeled by using a bent continuum potential; and (4) the wavelength for particle oscillation in its periodic motion is short compared to the length of the bent crystal. All of these assumptions are supported by extensive experimental studies on particles channeled over the energy range from a few KeV to 250 GeV.

To put this into experimental terms, Figure 10 gives several predictions for protons channeled along (111) planes in curved silicon crystals, with the abscissa expressed in terms of pv/R. This figure shows Kudo's calculation[48] for the wide and narrow (111) planes in silicon (with $a_T>0$, to give some indication of charge smearing effects), as well as corresponding curves from calculations by Ellison[49], using a weighted average of these wide and narrow planes in the case of the latter curves. Finally, another curve is shown, depicting Kudo's calculation for a parallel beam distribution incident on the wide planes. Recall that a curve lying further to the right indicates less bending dechanneling.

Note, first, that the effects of the wide planes and the narrow planes are reversed in the Ellison and the Kudo calculations. This may be due to the fact that Ellison uses fewer planes away from the channel in the potential calculation. The two sets are also not exactly comparable because different screening distances were used. When this is taken into account they are reasonably comparable. Notice, however, that the Kudo parallel incidence case is drastically different. Thus different choices of the potential, screening distances, and incident distributions can cause changes of almost a factor of two in the dechanneling probability.

As noted earlier, the distribution of electrons sampled in a bent crystal is different and denser than an unbent crystal because the trajectories are shifted closer to the nuclear planes. Vorobiev and his collaborators[31,50] have studied this behavior using several different electron densities in the Fokker-Planck equation. Figure 11 shows how the conventional dechanneling length drops for small radii of curvature. Figure 12 illustrates how this effect varies with energy.

V. Experimental Measurements of Ordinary Channeling

Two techniques are ordinarily employed for dechanneling studies; backscattering experiments and transmission measurements. Backscattering measurements are typically used at nuclear physics energies in the MeV regime because the ranges of the particles are on the order of tens to hundreds of microns. Conversely, at GeV energies transmission measurements are appropriate. Figure 13 illustrates these two techniques schematically. A useful discussion of the two approaches is contained in Grasso's article in Morgan's book on channeling[52].

Dechanneling measurements have been carried out for many different materials but only for silicon and germanium at high energy. For that reason this review concentrates on these two elements and tungsten. Tungsten is considered because of its potential for some practical applications at high energy.

In the backscattering technique the backscattering of the beam particle off of an atomic nucleus is observed. In a channeling direction this process is suppressed. The depth at which the interaction occurs is determined by measuring the recoil energy of the particle after the scattering. The

energy loss the particle has experienced consists of three parts; the energy loss while it was moving in a channel before the scattering, the energy lost to the recoil in a collision with a finite mass nucleus, and the energy loss afterward when it was moving in a random direction.

There is a problem in that the differential energy loss in the channel is smaller than in a random direction and also somewhat indeterminate. This leads to some uncertainty in the measurement of dechanneling by backscattering. (Davies et al.[13] estimates that this could alter the length scale by up to 12%.) To put this in perspective recall that the range of a proton in silicon in a random direction is approximately 17 microns at 1 MeV and 660 microns at 10 MeV. The corresponding planar dechanneling lengths are 2 microns and 20 microns.

Rather than extracting a dechanneling length, experiments in the MeV range are typically reported in terms of the dechanneled fraction as a function of depth (or energy loss). Often this functional dependence is non-exponential. It may also show the effects of an amorphous surface layer. In what follows the length extracted from the dechanneling fraction information will sometimes be called the half thickness for escape.

Feldman and Appleton[53] argue that the effect of energy

loss in such a situation does not make a substantial difference. They have measured half thicknesses for escape using backscattering with two different approaches to setting the energy loss and find agreement to within about 20%. Their results for the silicon (111) and (110) planes are illustrated in Figure 14.

Some transmission measurements of the dechanneling length have been made in the MeV regime. Feldman and Appleton[53] find agreement between the two methods to about 10% with the transmission results giving the smaller numbers.

There are other important differences between the MeV and the GeV regimes besides the fact that the GeV results principally use transmission measurements. At low energy the beam divergence is characteristically much smaller than the critical angle so that the initial condition for the diffusion calculation can be simpler. On the other hand many of these measurements at low energy were made fifteen to twenty years ago and there is usually no information reported that characterizes the material for defects and dislocations. Finally, in the multi-hundred GeV region dechanneling lengths are so large that it is difficult to obtain a crystal long enough to produce much dechanneling.

Figure 14 illustrates the linear energy dependence

expected from the diffusion equation. This has generally been confirmed for experiments in the 0.3[16] to 12 MeV range except for axial measurements reported in tungsten by Davies et al.[13,14] While they observed an energy dependence in the planar case they saw almost none in their axial measurements. No satisfactory explanation has been found for this particular result. One possibility might be the presence of some form of stacking fault in the crystal, although it is difficult to see how that would not affect the planar channeling.

Both planar and axial channeling at MeV energies are well fitted by diffusion model calculations. Figure 15 shows the Waho and Ohtsuki[20] dechanneling theory fit (as shown in Ohtsuki[18]) to the experimental values for planar channeling in silicon. The agreement is good. There is very little, if any, temperature dependence[16] for the planar case.

Figure 16 illustrates the result of a diffusion calculation fit to axial dechanneling in silicon[17]. Note that the temperature effect is obvious and well fitted for the model. (Parenthetically, Pedersen et al.[51] note that their silicon fits for this case do not agree with their experimental data at small depths.) Figure 17 shows axial channeling in tungsten. In this case the temperature dependence is not as well fitted, although Pedersen et al.[51] remark that it is. It

should be emphasized that the model fits shown in the last several figures are based on three different theoretical approaches that differ in many details.

These fits also demonstrate that the theoretical models fit the functional dependence on Z quite well. For example Pedersen at al.[51] find good fits to axial channeling at room temperature for both silicon and tungsten. Likewise they are able to reproduce the behavior as a function of different crystal geometries, that is to say, different axial orientations. Their data for different axial orientations in tungsten is given in Figure 18.

While most of these measurements are based on backscattering, the transmission experiments also reproduce the angular distribution of the transmitted particles. This is illustrated in Figure 19 taken from Pedersen et al.[51] for axial channeling in silicon and tungsten.

Tables II, III, and IV summarize much of the experimental information on the half thicknesses for escape in silicon, germanium, and tungsten. In some cases (marked g) the dechanneling lengths have been extracted from graphs of Chi-Chi_0 as a function of depth. Typically this was done at the highest point on the plot of Chi-Chi_0 where there was data. These Chi-Chi_0 values are given in brackets in Tables II-IV. This

technique is only approximate since in some cases these curves do not have an exponential form.

As noted earlier these measurements are generally in good agreement with model calculations except for the temperature and energy dependence of axial channeling and possibly the magnitude of the planar dechanneling length in tungsten. The early measurements of Davies et al.[13] appear to give shorter dechanneling lengths than graphical estimates based on their later work[14] and also the phenomenological formula (1).

One point may be worth noting. While almost none of these experiments quotes direct errors, the observations of Feldman and Appleton[53] suggest that the measurements should not be relied on to more than twenty percent. It is also true that most of these dechanneling measurements do not reach several e-foldings in the dechanneling process. This means the diffusion models may not be as strongly challenged by these results as they are by the high energy cases that will be discussed next.

In recent years experiments have been carried out to measure dechanneling lengths for silicon and germanium in the GeV regime. Several experimental approaches have been used. Transmission measurements have been performed, either employing different crystal thicknesses or by using energy

loss measurements in diodes implanted along the crystal to establish whether or not the particles were still channeled. A second attack has been to measure dechanneling in a gently bent crystal.

The principal problem with these determinations is that the beam angular distribution is often greater than the critical angle[31]. Using a bent crystal for dechanneling studies is also open to criticism since the dechanneling length should be shorter for the bent case. On the other hand there are no problems with energy loss in the material at high energy. In addition these experiments have generally been carried out with very good material. In at least one case, the Leningrad studies[47], that material has also been well characterized in regard to the interstitial and dislocation density.

There are relatively few measurements of dechanneling at GeV energies performed by directly varying the thickness of the crystal sample. In part this is due to the fact that the dechanneling lengths are becoming so long that very thick crystals are needed to get a 1/e folding length. (Note however, that the crystals used for bending measurements are sufficiently long to see appreciable dechanneling.) Jensen's thesis[54], however, does contain a comparison of measurements of axial dechanneling in germanium at 10 GeV/c to a diffusion

model. Two different thicknesses were measured. When the exit angular resolution was included, there was good agreement between the diffusion theory and experiment. The comparisons are shown in Figures 20 and 21. There is distinctly more dechanneling in the 4.0 mm case than for the 0.585 mm crystal.

An Albany-Lehigh-Fermilab-Dubna-UCLA group[55] has also looked at diffusion along the <110> axis in a 2cm germanium crystal. The energy was varied between 35 GeV and 250 GeV as an alternative to varying the crystal thickness. The behavior roughly followed the diffusion equation although there were more particles along the axis than predicted by the diffusion model. This may have been due to instrumental effects such as resolution or goniometer drift.

Forster and his colleagues[56] have measured dechanneling lengths for GeV energies by another technique that effectively mimics the process of using different crystal thicknesses. In this procedure a series of intrinsic diodes are implanted along a silicon strip. The energy loss in each of these detectors is measured. Channeled particles normally have substantially less energy loss in the detectors. Using this fact, channeled particles are tracked through the crystal to determine in which detector they dechannel. Dechanneling lengths were measured for the (110) plane in

silicon for energies ranging from 30 GeV to 200 GeV. The silicon was 50 kohm*cm n-type.

The measurements were well-fit by an exponential dechanneling picture. At 35 GeV the detector spacing was sufficient to see one e-fold. Two experiments were performed with different detector spacings. The two agree to within about twenty percent. These measurements are shown in Figure 22. In general they show a linear energy dependence. In detail there are a few problems. The 200 GeV point is somewhat low compared to a linear extrapolation, at least raising the possibility that there might be an incipient problem with crystal defects (see Section VII). The data also does not extrapolate to zero dechanneling length for zero energy.

Several groups have measured dechanneling lengths in gently bent crystals. Typically this is done by observing the dechanneling after the middle point of the bend in a so-called three point bending jig. Beyond that point the bending radius is increasing so there should be no further dechanneling due to the bending process itself. Sun et al.[57] used this approach at Dubna in the original bending experiment to get a dechanneling length for 8.4 Gev protons. They obtained a value of 8.6±0.5 mm for the (111) plane in silicon. This was for a crystal bent through angles of 4.7 mrad and 12 mrad over a 1 cm distance. Using this same technique, the CERN-

Aarhus group[46] estimates that the (110) planar dechanneling length for 12 GeV/c positive particles is approximately 8 mm. This was for a crystal bent through 20 mrad over a length on the order of 1 cm. Earlier, the same group had obtained a length that was found to be in good agreement with an estimate of 15 mm for 10 GeV/c protons[58]. The spread may give some sense of the challenges of this approach. All of these GeV regime results are tabulated in Tables IIa.

Both the data from the MeV and the GeV regime can be fit with a single formula. The kinematic variables must be treated relativistically and due consideration must be given to the incident beam distribution. This is done here by including a factor A_v, taken from Taratin and Vorobiev[31]. Here A_v is taken as 0.55 for dechanneling lengths in the GeV regime to account for the fact that such beams uniformly illuminate the channel. For the MeV regime A_v=1. The fitting formula for the dechanneling length is:

$$L(p)=L(p_0)*(pv/p_0v_0)*(A_v/A_{v0}) \qquad (8)$$

Here p,v are the momentum and velocity of the particle and $L(p_0)$ is a constant that is equivalent to a dechanneling length at a particular momentum. At MeV energies pv can be

replaced by 2T where T is the kinetic energy. For GeV energies pv=E, the total energy. Thus a raw extrapolation of the MeV lengths to the GeV regime without the kinematic term or A_v would give dechanneling lengths a factor of roughly four too long.

Information is available for Si(110) over a range from 0.3 MeV to 200 GeV. This data has been fitted for three data clusters: 1.3-8.9 MeV, 12-200 GeV, and 1.3 MeV-200 GeV. The fits were done as a simple one parameter average to equation (8) rather than a least squares analysis. Information on the fits is given in Table V. The fits are surprisingly good. The error is consistent with differences between different techniques (see, for example, the earlier comments from Feldman and Appleton[53]) and between individual measurements at different energies for the same experiment. The errors shown in Table V are one sigma. Fractional standard deviations from these fits are given in parentheses in Tables II-IV. Positive values indicate experimental dechanneling lengths that are larger than the fits.

Data below 1.3 MeV were not used because there is the possibility of a non-linear energy dependence due to the logarithmic term for the multiple scattering angle. Indeed, the fits are several standard deviations off from the experimental values for these low-energy points. The points above

30 GeV are consistently below the fitted line with the deviations increasing with increasing energy. As noted earlier, this might be due to either a problem with dislocations or a systematic problem with the measurements. Note, however, that this is only marginally significant at best. In general the fit is rather good considering it subsumes data gathered over an enormous range of energies with widely different techniques. Figure 23 shows all of the Si (110) experimental information along with the fitted curve for all energies.

Table V also gives fits for Si(111), Ge(110), W(110), and W(100). All of these are consistently well fit. Thus from the practical point of extrapolating to the TeV regime it appears that this information can be used with some confidence (perhaps to 20%), provided one is using perfect materials. Note however, that the planar tungsten fits may disagree with later work by the same group and the functional dependence of the phenomenological formula (1).

VI. Experiments on Bending Dechanneling

Several experiments have now been performed to explore the nature of dechanneling in bending. Details of these experiments can be found in the review article by Carrigan and Gibson[59]. Figure 24, taken from the Fermilab experiments[45], shows typical angular distributions for emergent particles from a three-point bending apparatus. This illustrates the bending distribution in the (111) planes of Si for several different energies. The figure focuses on particles that were channeled in the upstream (unbent) region of the crystal by selecting particles that exhibited low energy loss in the semiconductor detector. In every case there is a peak in the forward (undeflected) direction which is due, in part, to particles that dechannel before the bend. For 12 GeV and 60 GeV, there is also a prominent peak in a direction corresponding to the full deflection of the crystal. However for the 60 GeV case an intermediate peak can be seen at half the total bending angle. For angles somewhat beyond the middle peak but less than the full bend there are few particles, suggesting that the particles are well channeled between the middle and final peak. The middle peak is clearly associated with the middle pin in the three point bender. At 180 GeV both the intermediate and the full deflection peaks drop substantially. This indicates that the curvature is large

enough in this case so that a large fraction of the particles is being lost to bending dechanneling.

The magnitude of the peaks in the angular distribution as well as the intensity of the distribution of the particles between the peaks give important information on the dechanneling processes in bending. However, measuring the dechanneling in bending is complicated by several factors. Ordinary dechanneling occurs in the portion of the crystal after the detector and before the bend. Particles can also leak out of the sides of the detector if the planes are not perfectly aligned with the geometric sides of the crystal. Crystals bent with slowly increasing curvature should produce "bending" dechanneling only between the first and second pins of the bending apparatus[60]. No dechanneling is expected due to the bending or centrifugal effect in regions in which the curvature is constant or slowly decreasing. Such an effect is evident in the distributions shown in Figure 24. This appears as a larger emergent particle intensity between the first and second pins (1-2 mrad) compared to that between the second and third pins (5-6 mrad). This type of slowly-varying curvature is called "global curvature". The prominent intermediate peaks are not, however, predicted by global-curvature dechanneling effects.

From the Fermilab experiment, it is believed that the

origin of the intermediate peak is local curvature in the region of the middle pin in the three-point bending jig. The distortion is greatest on the crystal side near the pin and decreases gradually to zero on the side opposite the pin. Such dependence on the precise position of the particle trajectory in the crystal slab has been investigated directly, since the point of impact on the crystal could be determined from a drift chamber just in front of the crystal. With this it is possible to estimate the dechanneled fraction as a function of the position across the crystal by computing the ratio of the particles dechanneled at the pin divided by the sum of the particles that dechanneled plus the particles that continued on.

Using the local curvature or distortion calculated from classical elastic deformation theory, the dechanneling at the pin can be used as a "dechanneling spectrometer" to determine the dechanneling due to bending. This is called the "local curvature" method. This approach minimizes the effects of normal dechanneling and misalignment, since the bending losses occur in a small angular region and thereby a small fraction of the length of the crystal.

Figure 25 shows the channeling probability vs p/R. The results of continuum-model calculations by Ellison[49] are also shown for particles channeled between the (111) planes of

silicon. The curve to the right is for the wide planes with no charge smearing. The left curve includes charge smearing and is averaged over both wide and narrow planes. As noted earlier, the theoretical estimates are somewhat sensitive to the number of planes included in the potential and the assumed potential distribution[48]. The curvature was computed using a finite-element program as well as analytic approximations to the solutions of the differential equations for elastic deformations. The local distortion situation is actually quite complex. For example, the detailed shape of the pin contact may influence the distribution. Thus the absolute value of the abscissa is uncertain but the beam energy dependence should be good.

The apparent good agreement shown in Fig. 25 between the experimental measurements and the theory must be regarded as somewhat fortuitous because of approximations and averages contained in the "local curvature" analysis. The comparison should not, therefore, be regarded as justification for evaluating detailed differences between models. It does show that the continuum model technique gives the observed functional dependence and constitutes a reasonable basis for estimating the transmission of channeled particles through bent crystals. As expected, the "Tsyganov radius" approach seriously overestimates the particle transmission probability.

Observed particle losses between the bending pins, especially for small bending radii, can be used to establish "ordinary dechanneling" for the bending situation. When this is done, an interesting feature comes to light. For the Fermilab experiments for Si(111), the losses between the second and third pin give dechanneling lengths of 10 mm (12 GeV), 40 mm (30 GeV), 140 mm (60 GeV), 100 mm (100 GeV), and 30 mm (180 GeV). The 12 GeV result is consistent with the Dubna and CERN results. The 30 GeV and 60 GeV dechanneling lengths are also reasonably consistent with the Chalk River-Fermilab results given the limitations of the bending measurements. Above 60 GeV, the dechanneling lengths fall away from a linear extrapolation and even begin to decrease with energy. This diminution probably occurs because the trajectories are being forced ever closer to the sides of the channels, where they are subjected to higher charge densities and more dechanneling. Alternatively, the motion of the locus of the equilibrium points for the oscillatory motion toward the outside plane of the bend can be thought of as a reduction of the effective width of the planar channel.

VII. Defect Dechanneling

For high energy applications crystal defects probably represent the ultimate limitation on the use of channeling. By now applications at energies up to 20 TeV have been proposed[61]. At that energy the critical angle for Si (110) will be down to approximately one microradian. This is a very small angle indeed. On the other hand, channeling has already been observed up to 0.8 TeV, where the critical angle is only a factor of five larger.

The best crystal characterizations of silicon for channeling purposes appear to be due to the Leningrad group[47]. They estimate that their silicon had not more than 10-100 dislocations/cm^2 initially. However they note that the fabrication process could add dislocations. They used a two-crystal x-ray spectrometer to measure the line width of an x-ray line and thereby obtain an upper limit on the dislocation density. They found a line width of 2.6 seconds compared to the expected perfect crystal line width of 1.34 seconds. This number sets an upper limit on the dislocation density of 2000/cm^2. Surface etching indicated a surface density of 100/cm^2. They also looked at so-called A and B type clusters, corresponding to dislocation loops with radii of 1-3 and 0.06-0.8 microns respectively. The A type clusters dominate

the working portion of their crystal and have a density of less than $100/cm^2$.

Samsonov estimates the dechanneling length for the highest dislocation density to be 15 cm at 1 GeV. If we assume this extrapolates as the reciprocal of the square root of the energy (that is, inversely with the critical angle) then the normal dechanneling length will be equal to the dislocation dechanneling length at 26 GeV. For a dislocation density of $100/cm^2$ the two lengths will be equal at 200 GeV. This implies that even for very good silicon (say $10/cm^2$) there will be problems with dislocation dechanneling in the TeV regime.

Nevertheless there is reason for hope. The Samsonov cross sections may be unduly pessimistic. A lot of effort continues to go into producing ever higher quality silicon. Using the crystal characterization techniques employed by Samsonov, it is possible to select better portions of these "perfect" ingots. And finally, there are analysis techniques (Pendelosung fringes) that can measure dislocations at this level[62].

Going from a semiconductor to a metal when discussing defect dechanneling is like going from the sublime to the ridiculous. High Z materials such as tungsten have several

desirable features for possible high energy applications, including a large critical angle. The problem is that dislocation densities in these metals are very high compared to silicon. The lack of any energy dependence for the MeV axial channeling measurements in tungsten[13,14] may already be a hint of material problems. In this connection it should be noted that most of the MeV tungsten channeling measurements around the world were done with the same basic material sample.

Seeger[62] notes that growing metal crystals is considerably more difficult than growing semiconductors. He states that a really good tungsten or tantalum crystal might have a mosaic spread of several minutes (say 0.5 milliradians). Gibson[63] estimates that a very-good, currently-available tungsten crystal might have a mosaic spread of 0.01 degrees or 0.17 milliradians.This suggests that even the best currently-available tungsten crystals would fail in the region from 1-10 GeV.

The highest energy channeling measurements carried out with a tungsten crystal were done by a Sandia-Stanford-LLNL-Oak Ridge group[64]. They measured the channeling radiation for 83 MeV positrons for major planes and axes. The crystal was 100 microns thick and several mm transverse to the beam. They believe the crystal was among the best in the world.

Beezhold measured the mosaic spread of the crystal by comparing the x-ray diffraction pattern to a good silicon crystal and found the spread to be less than 0.9 milli-radians. The experimenters do note that the measured photon yields were not in perfect agreement with calculations.

In summary, at this point the defect limitations of very good tungsten crystals have not yet been challenged. They will probably be encountered in the 1-10 GeV regime.

VIII. Positron, Electron, and Heavy Negative Particle

The differences between heavy particle dechanneling and positron and electron dechanneling should be small. If a correct relativistic approach has been used it is only necessary to replace the ion scattering factor with the correct value for a positron or an electron and substitute the proper minimum and maximum electron or positron momenta transfers in the logarithmic terms of the multiple scattering treatment[18].

Three different lengths are discussed in connection with electron and positron channeling. There is the conventional dechanneling length, that is the distance for the particle to leave the channel. The second is an occupation length, or the distance over which two quantum states can be supported. This should be shorter than the dechanneling length but of roughly the same magnitude. In what follows the two terms are used interchangeably. Finally there is the coherence length, the distance over which radiation from the particle remains coherent. This length grows as the square of the total energy. It relates to the sharpness of the channeling radiation peaks, not the dechanneling length.

Wedell[65] has recently reviewed the theoretical picture for

electron and positron dechanneling. As with heavy particle dechanneling there are two basic approaches to treating the problem. The first is the Monte Carlo technique. The second is the diffusion approach. An example of the Monte Carlo attack is given in S. D. Bloom et al.[66] A problem with this method is that it requires long computer runs to get several e-foldings for the dechanneling process. In addition, each case must be approached with a new run so that it is complicated to study something like the functional dependence with energy.

As with the heavy particle case, the diffusion model is actually quite successful for positrons. Following this technique, Beloshitsky and Trikalinos[67] derived a positron planar dechanneling length of $z_{1/2}$=500 microns for the (110) plane of silicon at 1 GeV. Presumably this was for a beam with no initial angular divergence. This dechanneling length is within a factor of two of heavy particle calculations such as Ohtsuki[18].

The electron planar case is more difficult to treat. Quasichanneling is an important effect. In addition, there should also be a contribution due to lattice vibrations. Indeed, temperature effects due to lattice vibrations have been observed for planar electron channeling radiation spectra[68]. Wedell states that the electronic dechanneling

lengths are generally one order of magnitude smaller than the positron values. Some feeling for this is given in Figure 26 taken from Beloshitsky and Komarov[69]. There the Si (110) positron dechanneling length (1/e) is found to be approximately 700 microns at 1 GeV. The electron quasichanneling length for the same case is about 130 microns while the pure electron dechanneling length is 13 microns. All three of these are for a pencil beam parallel to the plane.

For the positron axial case the same techniques for scaling should hold that applied to the heavy particle situation. Again the negative case is more complicated. The angular momentum of the electron around an individual string must now be considered. This leads to a two-dimensional diffusion equation. Muralev[70] has treated this case. He obtains electron dechanneling lengths at 1 GeV and a temperature of 20 degrees Celsius for the <111> axis in Si of 13 microns, for Ge (7 microns), and for W (15 microns). He notes that the lengths scale slightly less rapidly than the normal linear energy dependence. However for practical purposes this is still a reasonable approximation. Taratin and Vorobiev[71] have also treated electron axial channeling using a numerical model. They obtain a maximum dechanneling length of $z_{1/2}$=18 microns for Si <111> at 1 GeV. This maximum occurs for particle trajectories at an angle of 0.36 of the critical angle. This is in fair agreement with Muralev.

The experimental information on electron and positron dechanneling is rather sparse. The most recent data seems to have been obtained by the Livermore-Stanford-Oak Ridge (LSO) group[72]. They have determined occupation lengths for silicon planar channeling by looking at particular transitions as a function of crystal thickness. Their results (1/e) are presented in Table VI. They estimate that the 60 micron value for Si(110) positron channeling is good to within 25 or 30%. Presumably these measurements are for a beam with an angular divergence much less than the critical angle. They find the dependence with thickness is definitely not exponential. They also find that the length does not grow linearly with the energy. Note that their electron lengths are roughly half of the positron lengths which is in disagreement with the theoretical predictions discussed earlier. One interesting feature is that they can tell the difference between different principal quantum states.

Komaki et al.[73] have obtained a dechanneling length (1/e) for Si (110) of 31 microns for 350 MeV electrons. This would be equivalent to a dechanneling length of 5 microns at 54 MeV and would seem to be in agreement with the theoretical calculations and in conflict with the measurements of LSO. At 1.2 GeV Adejshvili et al.[74] have measured a dechanneling length (1/e) of 28±5 microns for Si (110). This is substan-

tially lower than the theoretical estimates. Information from the measurements of Andersen et al.[75] suggests a dechanneling length on the order of 1 micron at 4 MeV for Si (110). This is more consistent with theory and the Komaki et al. value than with LSO. In summary, there is wide disagreement between the various experiments and also between some experiments and theory. One possible explanation for part of the disagreement may be that LSO also includes some aspect of quasichanneling behavior in their measurements.

The only experimental information on electron axial channeling appears to be the experiment of Adejshvili et al.[74] They have obtained a dechanneling length (1/e) of 39±4 microns for the <111> axis in silicon. Wedell states that this is in agreement with theory.

Information on negative heavy particle channeling is even more sparse. Andersen et al.[76] have looked at negative pion dechanneling at 15 GeV in germanium. For beam particles very close to the <110> axis they see transmissions of approximately 39% for a thickness of 0.3 mm, 27% for 0.7 mm, and 8% for 4.2 mm. It is not possible to fit these three values with a single reasonable dechanneling length. The value for the thickest crystal is really equivalent to the expected distribution for an amorphous crystal. If the amorphous distribution is subtracted from the other two, one obtains a

dechanneling length (1/e) of 0.3-0.5 mm. This is somewhat lower than the value for electron dechanneling scaled from Adejshvili et al.[74] at 1.2 GeV. Note that the thickest crystal in the Andersen et al. experiment is still too thin to expect any appreciable positive dechanneling at 15 GeV.

IX. Dechanneling Information Needed For The Future

The fundamentals of the theory of ordinary dechanneling are relatively well established. Diffusion-like models have the power to describe both heavy and light positive particle dechanneling for axial and planar geometries. The situation for negative particles is less clear, in part because of experimental uncertainties that will be discussed later.

From a practical standpoint there is a problem in that either a diffusion theory or a Monte Carlo calculation has to be particularized to a concrete situation. This means that it is not possible to readily scale to different orientations or crystals. It also makes it more difficult to incorporate more sophisticated processes such as defect dechanneling or the effects of bending. The availability of a flexible phenomenological theory, well-rooted in a more fundamental picture, would be valuable.

There are theories of negative particle dechanneling. However, because of the fact that the experimental picture is so confused, it is difficult to judge how sound these are. Some of the differences in the reported experimental values may be related to theoretical considerations. For example,

some experiments may be reporting quasi-dechanneling lengths which should be substantially longer. As the experimental picture clarifies it can be expected that additional demands may be made on theory. Obviously more experimental information is desirable. In this regard negative axial heavy particle channeling in the multi-hundred GeV regime may be an interesting subject to pursue. At these energies the dechanneling length is becoming long enough that reasonably thick crystals could be used. Such information would be complementary to the confusing picture for electron dechanneling.

More work is needed on the theory of bending dechanneling. For example, there are differences between the results obtained by Kudo[48] and Ellison[49] that would seem to be due to different choices for charge distributions. These appear to give rise to substantially different bending effects for different crystal orientations. These differences should be resolved. In addition, the theory of ordinary dechanneling in bending needs to be refined beyond the early calculations of Taratin and Vorobiev[31]. In particular, their theory assumes a uniform distribution of valence electrons. It would be informative to try a better approximation. One interesting facet of ordinary dechanneling in bending is that it opens up the possibility of "designer dechanneling lengths". The bend can be used to control the potential that the particle moves in. It would be useful to understand whether this could

provide unique information about crystal potentials.

The theory of defect dechanneling appears to be satisfactory based on results at nuclear physics energies. However it is not so clear just how precise the theory is. It has not yet been confronted by the two pressing problems on the horizon for high energy applications; tungsten and silicon perfection. Indeed, silicon channeling in the trans-TeV region may well be the most challenging goal for crystal perfection studies now in sight. It is also important that a defect dechanneling theory be soundly linked to defect characterization, both experimentally and theoretically.

Planar dechanneling for positive particles in silicon has now been thoroughly explored over a range of nearly six decades in energy. The agreement among experiments and with the theory is quite good. As noted earlier, there are tiny hints of incipient trouble at the highest energies. This suggests further experiments at Tevatron energies to measure silicon dechanneling more accurately. Such experiments would require carefully characterized crystals. It would also be desirable to more have germanium measurements at GeV energies to confirm the silicon behavior with another well-characterized material.

Axial dechanneling for positive particles is not so well

understood. There is little concrete information at GeV energies because the dechanneling lengths are so long and because the bending and feeding-out studies have concentrated on the planar case. More information could be used on GeV axial channeling. Even at MeV energies there has been little direct study of the behavior with energy. However it is true that planar and axial dechanneling both usually follow theoretical predictions with the exception of tungsten.

For tungsten the experiments of Davies et al.[13] show almost no energy dependence for axial dechanneling in the MeV regime. There is also a hint of a problem in the tungsten planar results in that the earlier Davies et al.[13] experiment gives shorter dechanneling lengths than their later data[14] and phenomenological estimates. It seems quite unlikely that this indicates any fundamental difficulty. What is more probable is that there was some problem with crystal perfection. Since tungsten is a particularly favorable crystal for GeV channeling in other respects it would be very desirable to understand this situation. Specifically, it would be helpful to have a remeasurement for tungsten in the MeV regime. As noted earlier, experimental measurements of channeling in tungsten extend only up to 83 MeV while defect limitations are expected to set in in the 1-10 GeV regime. Measurements should be carried out at increasingly higher energies to the point of determining the limiting energy for

channeling. Obviously it is also important to pursue the quest for better high Z crystals.

Finally the exotic crystals mentioned at the beginning of the article may be important for futuristic applications of the channeling process. They offer rich possibilities for dechanneling studies over all energy ranges. The first work should probably be in the MeV regime.

ACKNOWLEDGEMENTS

The author is grateful to his colleagues for much help, instruction, and advice in the course of preparing this material. I would particularly like to acknowledge S. Baker (Fermilab), J. Ellison (New Mexico), J. Forster (Chalk River), W. Gibson (SUNY-Albany), R. Noble (Fermilab), S. Salman (Al Najah), C. Sun (SUNY-Albany), and R. Wijayawardana (Peradeniya).

Figures

1. Comparison of diffusion coefficients due to Lindhard and to Waho and Ohtsuki[20] for 4.8 MeV He^+ in Si(110). (Taken from Ohtsuki[18].)

2. Detailed profile of $D_{Y(E_Y)}$ for 4.8 MeV H^+ in Ge(110) according to Waho and Ohtsuki[20] and Kitagawa and Ohtsuki[21] showing the electronic and the nuclear contributions. (Taken from Ohtsuki[18].)

3. Modulation of the dechanneling length as a function of beam angular divergence normalized to the critical angle. The curves are universal and hold for any material. The numbers correspond to: (1) a straight channel, (2) a channel with $R=5R_T$, (3) $R=2R_T$. Taken from Taratin and Vorobiev[31].

4. Experimentally measured dechanneling factor for silicon as a function of the square root of the beam energy divided by the beam atomic number for (110) and <111> dechanneling in Si with a network of edge dislocations. From Picraux et al.[33]

5. Schematic of the energy dependence of the dechanneling

factors of various types of defects. From FMP[1].

6. Planar potential for 10 GeV protons moving in a silicon crystal for the (110) plane. The bending radius is 10 cm. The original potential W(y) is modified by the addition of a centrifugal potential. Taken from Kudo[48].

7. Schematics of channeled planar orbits in an unbent (a) and a bent (b) crystal. Note that the center of gravity of the orbit moves toward the outer plane in the bent crystal. Based in part on Ellison[49].

8. Typical phase space geometry for particles moving in a bent crystal for the wide (111) planes in silicon. x_c is the normalized distance to the charge plane, Psi is a normalized angle relative to the local plane direction, and x_e is the center line of the displaced trajectory. Particles in the inner ovals remain channeled while those in the cross-hatched region are lost. From Ellison[49].

9. Dechanneled fraction F versus the dimensionless parameter Gamma. Note that Gamma is proportional to the product of momentum and velocity divided by the radius of curvature. The values of x_c correspond to dechanneling at the planes and at the Thomas-Fermi screening distance away from the planes. C_F shows the point corresponding to the Tsyganov

radius. From Ellison[49].

10. Different calculations for the wide (L) and narrow (S)(111) planes in silicon. (---) Si (111)-S,L shown are Kudo's results[48] with a finite a_T value and an incident flux in statistical equilibrium; (- - -) is a similar case for the wide planes with a parallel incident flux. Kudo's calculation for Si (110) (---) in statistical equilibrium is also shown. (....) is Ellison's result[34] with no charge smearing and a weighted distribution of planes. The open circles and the open squares are Ellison's calculations for the wide and narrow planes, respectively. The dechanneling probability is in percent.

11. Dependence of the conventional dechanneling length ($x_{1/2}$ in millimeters) on the radius of curvature for the (110) plane in silicon for E=10 GeV (1) and 20 GeV (2) particles based on an averaged electron density . Case (3) shows a more realistic potential for 10 GeV. The figure is taken from Taratin, et al.[50] with the y axis multiplied by 6.28 to reflect only dechanneling by the valence electrons as discussed in Taratin and Vorobiev[31].

12. Conventional dechanneling half length as a function of energy for Si (110). (1) is for a straight channel, (2) for R=1 m, (3) for R=0.1 m. The figure is from Taratin and

Vorobiev[31].

13. Schematic illustration of the backscattering and transmission technique for measuring dechanneling. The energy spectrum labeled R and A correspond to random and aligned respectively.From Pedersen et al.[51]

14. Comparison for half thicknesses of escape in silicon determined by transmission measurements and by back-scattering. The heavy solid lines are the transmission measurements. From Feldman and Appleton[53].

15. Experimental values for half thicknesses for escape compared to dechanneling theory for Si(110). The theoretical predictions for Ge (110) are also shown. Taken from Ohtsuki[18].

16. Matsunami and Howe[17] diffusion model fit to <110> axial dechanneling in silicon. Note that the strong temperature effect is well fit by the model.

17. Fit to <100> axial dechanneling in tungsten as a function of temperature. Note that the temperature effect is not as well fitted as it was in silicon. From Pedersen et al.[51]

18. Measured dechanneling for tungsten in different axial

orientations for a beam energy of 2 MeV compared to the Schiott et al.[15] model. From Pedersen et al.[51]

19. Measured angular distributions (points) for axial channeling in Si and W compared to Schiott et al.[15] model. From Pedersen et al.[51]

20. Comparison of measured exit distribution for 10 GeV/c protons transmitted through a 0.585 mm thick germanium crystal parallel to the <110> axis. Each panel shows a different interval of the incident angular distribution out to the critical angle. The solid curves in a) and b) show the theoretical distribution without (1) and with (2) the contribution of exit angular resolution. In c) an d) the solid curves do not include the angular resolution. From Jensen[54].

21. Same as figure 20 but for a 4.0 mm germanium crystal. The solid curves are calculated from a diffusion model without experimental resolution effects. From Jensen[54].

22. Feeding-out lengths (1/e) determined in the Chalk River-Fermilab experiment[56]. The open and closed triangles represent two different experiments with different detector spacings.

23. Behavior of the ordinary dechanneling length (1/e) for Si (110) as a function of kinetic energy. (The points in the GeV regime are plotted at momentum values since they are for mixed beams. There is only a small error in doing this.) Three curves are shown: the solid curve is based on the Ohtsuki diffusion length[18] extrapolated for pions, the dashed curve for protons, and the double dashed curve is the empirical fit to all energies including the effects of a broadly illuminated channel in the GeV range. In the MeV regime this fit lies on the Ohtsuki line and is not shown. The dots are Campisano et al.[16], the crosses are Feldman and Appleton[53], the diamond is Davies et al.[13], the CERN point is Bak et al.[46], and the Fermilab data is Forster[56].

24. Distribution of outgoing particle directions in the Fermilab bending experiment with a small energy loss cut in the detector. The crystal bend is 8 milliradians and incident energies are 12, 60, and 180 Gev(a-c). The peak at 0 milliradians, the beam direction, is due mostly to particles dechanneled prior to the first bend. Note the peak at approximately 4 milliradians that develops as the energy is increased.

25. Comparison of the dechanneling fraction as a function of the momentum divided by the radius of curvature. The theoretical curves are taken from Ellison[49] for the (111)

planes in silicon. The right curve is for the wide planes with no charge smearing while the left curve includes charge smearing and is averaged over planes. Experimental points are based on the losses at the middle pin in the three-point bender. The point predicted by the Tsyganov centrifugal-force calculation for the charge smeared case is indicated by CF.

26. Dechanneling fraction for proper channeled particles (with $E_{tran}<U_m$) and quasichanneled particles (with $E_{tran}<4U_m$) at different incident angles and energies as a function of the crystal depth in microns divided by the energy in GeV. a) for positrons in Si (110) with the solid lines representing the channeled fraction and the dash-dot lines the quasichanneled fraction at 100 MeV; the dashed line the dechanneled fraction at 1 GeV and the dotted line the dechanneled fraction at 10 GeV. b) for electrons in Si (110) with the upper curves presenting the proper channeled fraction and the lower curves the quasichanneled fraction. The solid lines show the case for the incident angle equal to the critical angle while the dashed lines are for the case of the incident angle equal to zero. Panel b) is for the energy interval $1<E<10$ GeV. From Beloshitsky and Komarov[69].

Bibliography

1. L. C. Feldman, J. W. Mayer, S. T. Picraux, "Materials Analysis by Ion Channeling", Academic Press, New York (1982).
2. H. E. Schiott in Relativistic Channeling, R. A. Carrigan, Jr. and J. A. Ellison, Ed. (Plenum, New York), to be published.
3. J. Lindhard Mat.-fys. Med. Kog. Dan. Vid. Sel. 34, no. 14(1965).
4. E. Bonderup, H. Esbensen, J. U. Andersen, and H. E. Schiott, Rad. Effects 12, 261 (1972).
5. W. K. Chu, J. A. Ellison, S. T. Picraux, R. M. Biefeld, G C. Osborne, Phys. Rev. Lett. 52, 125 (1984).
6. G. Gruner and A. Zettl, Phys. Rep. 119, 117 (1985).
7. B. S. Elman, G. Braunstein, M. S. Dresselhaus, and G.Dresselhaus, T. Venkatesan, and B. Wilkens, J. Appl. Phys. 56, 2114 (1984), D. Schroyen, M.Bruggeman, I. Dezsi, and G. Langouche, Nucl. Instr. and Meth. B15, 341(1986).
8. J. M. Newsam, Science 231, 1093 (1986).
9. S. I. Baker, R. A. Carrigan, Jr., R. Schailey, T. E. Toohig, W. M. Gibson, I.-J. Kim, F. Sun, C. R. Sun, V. Tanikella, R. Wijayawardana, J. S. Forster, H. Hatton, I. V. Mitchell, and J. A. Ellison, Nucl. Instr. and Meth. A234, 602 (1985), S. I. Baker, R. A. Carrigan, Jr., R. L.

Dixon, H. C. Fenker, R. J. Stefanski, J. S. Forster, R. L. Wijayawardana, and S. Reucroft, Nucl. Instr. and Meth. A248, 301(1986), R. L. Wijayawardana, Thesis, State University of New York-Albany(1985).

10. P. Chen and R. J. Noble, SLAC-PUB-4042 (1986). P. Chen and R. J. Noble in Relativistic Channeling, R. A. Carrigan, Jr. and J. A. Ellison, Ed. (Plenum, New York), to be published.
11. L. C. Feldman, B. R. Appleton, and W.L. Brown, Solid State Physics Research With Accelerators, Brookhaven National Laboratory Report No. BNL-50083, p. 58 (1968). (See also Feldman and Appleton[53].)
12. D. S. Gemmell, Reviews of Modern Physics, 46, 129 (1974).
13. J. A. Davies, J. Denhartog, and J. L. Whitton, Phys. Rev. 165, 345 (1968).
14. J. A. Davies, L. M. Howe, D. A. Marsden, and J. L. Whitton , Radiation Effects 12, 247 (1972).
15. H. E. Schiott, E. Bonderup, J. U. Andersen, and H. Esbensen, Atomic Collisions in Solids, Eds. S. Datz, B. R. Appleton, and C. D. Moak, Plenum ,New York(1975),p. 843.
16. S. U. Campisano, G. Foti, F. Grasso, M. Lo Savio, and E. Rimini, Radiation Effects 13, 157(1972) and earlier works.
17. N. Matsunami and L. M. Howe, Radiation Effects, 51, 111 (1980).
18. Y. H. Ohtsuki, Charged Beam Interaction With Solids,

Taylor and Francis-London (1983).

19. C. Ellegard and N. O. Lassen, Kgl. Dan. Viden. Sels. Mat-fys. Medd. 35, No. 16(1967).
20. T. Waho and Y. H. Ohtsuki, Radiation Effects,21,217 (1974).
21. M. Kitagawa and Y. H. Ohtsuki, Phys. Rev. B8, 3117 (1973).
22. H. Nitta, Quantum Theory of Local Diffusion Coefficient and Stopping Power for Channeled Particles, Thesis, Waseda University (1987).
23. M. A. Kumakhov and R. Wedell, Radiation Effects 30, 1 (1976).
24. K. Gärtner, K. Hehl, And G. Schlotzhauer, Nucl. Instr. and Methods 216, 275 (1983).
25. K. Gärtner, K. Hehl, And G. Schlotzhauer, Nucl. Instr. and Methods B4, 55 (1984).
26. K. Gärtner, K. Hehl, And G. Schlotzhauer, Nucl. Instr. and Methods B4, 63 (1984).
27. K. Gärtner and K. Hehl, Nucl. Instr. and Methods B12, 205 (1985).
28. K. Gärtner, G. Götz, and K. Hehl, Nucl. Instr. and Methods B2, 737 (1984).
29. T. Oshiyama and M-h. Mannami, Phys. Lett. 81A, 43 (1981).
30. V. V. Beloshitsky, M. A. Kumakhov, and V. A. Muralev, Rad. Eff. 13, 9 (1972).
31. A. M. Taratin and S. A. Vorobiev, Phys. Stat. Sol.(b)

107, 521 (1981).

32. Y. Quere, Phys. Status Solidi,30,713 (1968).

33. S. T. Picraux, J. A. Knapp, and E. Rimini (1982), as cited in FMP[1].

34. J. A. Ellison and S. T. Picraux, Phys. Lett. 83A, 271 (1981).

35. H. Kudo, J. Phys. Soc. Jap. 40, 1645(1976).

36. H. Kudo, Phys. Rev. B18, 5995 (1978).

37. L. Wielunski, D. Wielunska, G. Della Mea, and A. Turos, Nucl. Instr. and Meth. 168,323(1980).

38. D. Wielunska, L. Wielunski, and A. Turos, Phys. Status Solidi. (a)67, 413 (1981).

39. W. Zakowicz and R. H. Pantell, J. Appl. Phys. 52, 2799 (1981).

40. S.T. Picraux, W. K. Chu, W. R. Allen, and J. A. Ellison, Nucl. Instr. and Meth. B15, 306(1986).

41. E. N. Tsyganov, Fermilab TM-682, TM-684, Batavia, 1976.

42. A. F. Elishnev, N. A. Filatova, V. M. Golovatyuk, I. M. Ivanchenko, R. B. Kadyrov, N. N. Karpenko, V. V. Korenkov, T. S. Nigmanov, V. D. Riabtsov, M. D. Shafranov, B. Sitar, A. E. Senner, B. M. Starchenko, V. A. Sutulin, I. A. Tyapkin, E. N. Tsyganov, D. V. Uralsky, A. S. Vodopianov, A. Forycki, Z. Guzik, J. Wojtkowska, R. Zelazny, I. A. Grishaev, G. D. Kovalenko, B. I. Shramenko, M. D. Bavizhev, N. K. Bulgakov, V. V. Avdeichikov, R. A. Carrigan, Jr., T. E. Toohig, W. M.

Gibson, I-J. Kim, J. Phelps, And C. R. Sun, Physics Letters,88B, 387 (1979).

43. W. M. Gibson, I. J. Kim, M. Pisharody, S. M. Salman, C. R. Sun, G. H. Wang, R. Wijawaradana, J. S. Forster, I. V. Mitchell, T. S. Nigmanov, E. N. Tsyganov, S. I. Baker, R. A. Carrigan, T. E. Toohig, V. V. Avdeichikov, J. A. Ellison, P. Siffert, Nucl. Instr. and Meth. B2, 54 (1984).

44. S. I. Baker, R. A. Carrigan, C. Crawford, T. E. Toohig, W. M. Gibson, H. Jin, I. J. Kim, M. Pisharody, S. Salman, C. R. Sun, G. H. Wang, R. Wijawaradana, J. S. Forster, H. Hatton, I. V. Mitchell, Z. Guzik, T. S. Nigmanov, E. N. Tsyganov, V. V. Avdeichikov, J. A. Ellison, P. Siffert, Phys. Lett. 137B, 129 (1984).

45. S. M. Salman: Thesis, State University of New York (1982).

46. J. F. Bak, P. R. Jensen, H. Madsboll, S. P. Moller, H. E. Schiott, E. Uggerhoj, J.J. Grob, and P. Siffert, Nuclear Physics, B242, 1 (1984).

47. V. M. Samsonov, Relativistic Channeling, R. A. Carrigan, Jr. and J. A. Ellison, Ed. (Plenum, New York), to be published.

48. H. Kudo, Nucl. Instr. Meth. 189, 609 (1981).

49. J. A. Ellison, Nucl. Phys. B206, 205 (1982).

50. A. M. Taratin, Yu. M. Filomonov, E. G. Vyatkin, and S. A. Vorobiev, Phys. Status Solidi. (b)100, 273(1980).

51. M. J. Pedersen, J. U. Andersen, D. J. Elliott, and E. Laegsgaard, Atomic Collisions in Solids, Eds. S. Datz, B. R. Appleton, and C. D. Moak, Plenum ,New York(1975),p. 863.

52. "Channeling", D. V. Morgan, Ed., Wiley (1973).

53. L. C. Feldman and B. R. Appleton, Phys. Rev. B8, 935 (1973). (See also Feldman at al.[11]).

54. P. R. Jensen, Thesis, Aarhus, 1980.

55. C. R. Sun, W. M. Gibson, I. J. Kim, G. O. Williams, M. A. Hasan, A. S. Kanofsky, R. Allen, R. A. Carrigan, Jr., B. L. Chrisman, T. E. Toohig, Z. Guzik, T. S. Nigmanov, E. N. Tsyganov, A. S. Vodopianov, A. B. Watson, J. Kubic, And D. H. Stork, Nuclear Physics B203, 40 (1982).

56. J. S. Forster, Relativistic Channeling, R. A. Carrigan, Jr. and J. A. Ellison, Ed. (Plenum, New York), to be published.

57. C. R. Sun, W. M. Gibson, I. J. Kim, G. H. Wang, N. K. Bulganov, N. A. Filatova, A. Forycki, V. M. Golovatyuk,Z. Guzik, R. B. Kadyrov, T. S. Nigmanov, V. D. Riabtsov, A. B. Sadovsky, M. D. Shafranov, I. A. Tyapkin, E. N. Tsyganov, A. S. Vodopianov, J. Wojtkowska, A. Forycki, J. Wojtkowska, N. I. Zimin, R. A. Carrigan, Jr., T. E. Toohig, M. D. Bavizhev, Nucl. Instr. and Meth. B2, 60 (1984).

58. J. Bak, G. Melchart, E. Uggerhoj, J. S. Forster, P. R. Jensen, H. Madsboll, S. P. Moller, H. Nielsen, G.

Petersen, H. Schiott, J. J. Grob, and P. Siffert, Phys. Lett. 93B, 505 (1980).

59. R. A. Carrigan, Jr. and W. M. Gibson, p. 61, Coherent Radiation Sources, Eds. A.W. Saenz and H. Uberall, Springer-Verlag, Berlin (1985).

60. J. A. Ellison, S. I. Baker, R. A. Carrigan, Jr., J. S. Forster, I. V. Mitchell, W. M. Gibson, I. J. Kim, M. Pisharody, S. Salman, C. R. Sun, R. Wijawaradana, Nucl. Instr. and Meth. B2, 9 (1984).

61. C. R. Sun, R. A. Carrigan, Jr., T. E. Toohig, and D. Neuffer, Proceedings of the 1984 Summer Study on the Design and Utilization of the SSC (1984).

62. A. Seeger, Relativistic Channeling, R. A. Carrigan, Jr. and J. A. Ellison, Ed. (Plenum, New York), to be published.

63. W. M. Gibson, private communication.

64. W. Beezhold, T. W. L. Sanford, H. Park, J. O. Kephart, R. K. Klein, R. H. Pantell, B. L. Berman, and S. Datz, Bull. Am. Phys. Soc. 30, 374 (1985). W. Beezhold, private communication.

65. R. Wedell, Relativistic Channeling, R. A. Carrigan, Jr. and J. A. Ellison, Ed. (Plenum, New York), to be published.

66. S. D. Bloom, B.L. Berman, D. C. Hamilton, M. J. Alguard, J. H. Barrett, S. Datz, R. H. Pantell, and R.L. Swent, Nucl. Instr. and Meth. 194, 229 (1984).

67. V. V. Belotshitsky and Ch. Trikalinos, Rad. Eff. 56, 71 (1981).

68. R. L. Swent, R. H. Pantell, S. Datz, and R. Alvarez, Nucl. Instr. and Meth. 194, 235 (1982).

69. V. V. Belotshitsky and F. F. Komarov, Physics Reports 93, 117 (1982).

70. V. A. Muralev, Nucl. Instr. and Meth. B2, 51 (1984).

71. A. M. Taratin and S. A. Vorobiev, Phys. Stat. Sol. 124, 641 (1984).

72. B. L. Berman, Relativistic Channeling, R. A. Carrigan, Jr. and J. A. Ellison, Ed. (Plenum, New York), to be published. J. O. Kephart, private communication.

73. K. Komaki, A. Otuka, F. Fujimoto, N. Horikawa, T. Nakanishi, G. Y. Gao, T. Iwata, S. Fukui, M. Mutou, and K. Okuno, Nucl. Instr. and Methods B2, 71 (1984).

74. D. I. Adejshvili, G. B. Bochek, V. I. Vit'ko, G. D. Kovalenko, B. I. Shramenko, Rad. Eff. Let.,87, 135 (1985).

75. J. U. Andersen, E. Bonderup, and E. Laegsgaard, Coherent Radiation Sources, Eds. A.W. Saenz and H. Uberall, Springer-Verlag, Berlin (1985).

76. S. K. Andersen, O. Fich, H. Nielsen, H. E. Schiott, E. Uggerhoj, C. Vraast Thomsen, G. Charpak, G. Petersen, F. Sauli, J. P. Ponpon, and P. Siffert, Nucl. Phys. B167, 1 (1980).

TABLE I

Defect Dechanneling Factor σ_D and Densities n_D.
(From Feldman et al.[1])

Defect	Class	Dechanneling Factor σ_D (units)	Defect Density n_D (units)
Interstitial	Point	Area (cm^2)	Number/unit volume (cm^{-3})
Dislocation	Line	Area/defect length (cm)	Proj.length/unit vol. (cm^{-2})
Stacking fault	Area	Area/defect area (--)	Proj. area/unit vol. (cm^{-1})
Twin	Volume	Area/defect volume (cm^{-1})	Defect vol./unit vol. (--)

TABLE IIa

Silicon Hadronic Dechanneling Lengths For
Heavy Positive Particles in the MeV Regime

(These are half lengths in microns)

Energy	Axial			Planar			Temp	Method	Reference
	<100>	<110>	<111>	(100)	(110)	(111)	(Cel)		
0.3 MeV					0.8(3.3)			B. S.	Camp. et al.[16]
0.5 MeV					1.3A(3.1)	1.8A(2.0)	-193?	B. S.	Feld. & Ap.[53]
0.6 MeV					1.3(1.5)			B. S.	Camp. et al.[16]
1.0 MeV					2.2A(1.6)	3.0A(0.6)	-193?	B. S.	Feld. & Ap.[53]
1.0 MeV					2.0(0.8)			B. S.	Camp. et al.[16]
1.3 MeV					*2.95(1.8)	*4.0(.8)	-193?	Trans.	Feld. & Ap.[53]
1.5 MeV					*2.4(-0.6)			B. S.	Camp. et al.[16]
1.5 MeV					*3.2A(1.3)	*4.4A(.4)	-193?	B. S.	Feld. & Ap.[53]
1.6 MeV		22g[.22]					20	B. S.	Peder. et al.[51]
		14g[.32]					200	B. S.	Peder. et al.[51]
		11g[.40]					400	B. S.	Peder. et al.[51]
		8.5g[.48]					700	B. S.	Peder. et al.[51]
2.0 MeV					*4.2A(1.2)	*5.4A(.3)	-193?	B. S.	Feld. & Ap.[53]
2.8 MeV					*4.9(-0.1)	*8.3(.5)	-193?	Trans.	Feld. & Ap.[53]
3.0 MeV		11		2.3	*4.5(-1.0)	*5.0(-2.6)	25	B. S.	Davies et al.[13]
		8.6		2.1		4.7(-2.8)	250	B. S.	Davies et al.[13]
		8.0			3.7(-1.6)	4.0(-3.4)	350	B. S.	Davies et al.[13]
		7.3			4.0(-1.6)	4.8(-2.7)	500	B. S.	Davies et al.[13]
4.8 MeV					*9.3(0.6)	*13.8(.3)	-193?	Trans.	Feld. & Ap.[53]
4.9 MeV					*8.9(0.2)		-193?	Trans.	Feld. & Ap.[53]
6.9 MeV					*13.0(0.4)		-193?	Trans.	Feld. & Ap.[53]
8.9 MeV					*16.6(0.3)	*25.3(.2)	-193?	Trans.	Feld. & Ap.[53]

A= averaged over two energy loss techniques (Feld. & Ap.[53])
g:extracted from graph, * used in fits,
( ) indicate fractional standard deviations
[ ] point on Chi-Chi_0 graph used to extract dechanneling length

TABLE IIb

Silicon Hadronic Dechanneling Lengths For
Heavy Positive Particles in the GeV Regime

(These are 1/e lengths in millimeters)

Energy	Axial			Planar			Temp	Method	Reference
	<100>	<110>	<111>	(100)	(110)	(111)	(Cel)		
1.0 GeV						*1.26±0.9(1.0)	27	MD,Bend	Samsonov et al.[47]
8.4 GeV						*8.6±0.5(-.4)		Bend	Sun et al.[57]
12 GeV					*8(-0.3)			Bend	Bak et al.[46]
30 GeV					*22(0.3)		20	MD	Forster [56]
60 GeV					*36(-0.1)		20	MD	Forster [56]
100 GeV					*55(-1.4)		20	MD	Forster [56]
200 GeV					*103(-1.7)		20	MD	Forster [56]

* used in fits,
( ) indicate fractional standard deviations

TABLE III

Germanium Hadronic Dechanneling Lengths For
Heavy Positive Particles

(These are half lengths in microns)

Energy	Axial			Planar			Temp	Method	Reference
	<100>	<110>	<111>	(100)	(110)	(111)	(Cel)		
0.3 MeV					0.7(5.4)			B. S.	Camp. et al.[16]
0.3 MeV		7.1g[.11]	5.5g[.14]				22	B. S.	Mat. & Howe[17]
0.6 MeV					1.0(1.0)			B. S.	Camp. et al.[16]
0.6 MeV		10g[.18]	7.1g[.24]				22	B. S.	Mat. & Howe[17]
1.0 MeV					*1.4(-.8)			B. S.	Camp. et al.[16]
1.0 MeV		53g[.07]	29g[.12]				-233	B. S.	Mat. & Howe[17]
1.0 MeV		33g[.11]					-153	B. S.	Mat. & Howe[17]
1.0 MeV		22g[.16]					-73	B. S.	Mat. & Howe[17]
1.0 MeV		14g[.24]					7	B. S.	Mat. & Howe[17]
1.0 MeV			9.7g[.32]				-93	B. S.	Mat. & Howe[17]
1.0 MeV			8.8g[.36]				-17	B. S.	Mat. & Howe[17]
1.5 MeV					*2.0(-1.3)			B. S.	Camp. et al.[16]
1.5 MeV			31g[.20]				-233	B. S.	Mat. & Howe[17]
1.5 MeV			21g[.28]				-183	B. S.	Mat. & Howe[17]
1.5 MeV			14g[.39]				-113	B. S.	Mat. & Howe[17]
1.5 MeV			12g[.45]				-53	B. S.	Mat. & Howe[17]
1.5 MeV		12g[.44]	11g[.47]				22	B. S.	Mat. & Howe[17]
2.5 MeV			34g[.30]				-233	B. S.	Mat. & Howe[17]
2.5 MeV			25g[.38]				-183	B. S.	Mat. & Howe[17]
2.5 MeV			18g[.48]				-113	B. S.	Mat. & Howe[17]
2.5 MeV			15g[.55]				-53	B. S.	Mat. & Howe[17]
2.5 MeV			15g[.56]				22	B. S.	Mat. & Howe[17]
2.8 MeV					*4.8(1.3)	8.8	-193?	Trans	Feld. & Ap.[53]
4.8 MeV					*8.0(1.0)	12.2	-193?	Trans	Feld. & Ap.[53]
6.9 MeV					*9.7(-.8)	10.8	-193?	Trans	Feld. & Ap.[53]
8.9 MeV					*14.5(.7)		-193?	Trans	Feld. & Ap.[53]

g:extracted from graph, * used in fits,
( ) indicate fractional standard deviations
[ ] point on Chi-Chi_0 graph used to extract dechanneling length

TABLE IV

Tungsten Hadronic Dechanneling Lengths For
Heavy Positive Particles

(These are half lengths in microns)

Energy	Axial			Planar			Temp	Method	Reference
	<100>	<110>	<111>	(100)	(110)	(111)	(Cel)		
0.5 MeV					2.4g[.21]			B. S.	Davies et al.[14]
2.0 MeV	20			*1.3(-.8)	*2.7(-.9)		25	B. S.	Davies et al.[13]
2.0 MeV	57g[.05]						20	B. S.	Peder. et al.[51]
	35g[.08]						175	B. S.	Peder. et al.[51]
	23g[.12]						400	B. S.	Peder. et al.[51]
	11.3g[.23]						700	B. S.	Peder. et al.[51]
2.0 MeV			43g[.1]		5.6g[.5]			B. S.	Davies et al.[14]
3.0 MeV	23		44	*2.8(1.4)	*4.1(-.5)		25	B. S.	Davies et al.[13]
	17			2.7(1.2)	3.7(-3.1)		250	B. S.	Davies et al.[13]
	12			2.3(0.1)	3.5(-4.4)		450	B. S.	Davies et al.[13]
3.5 MeV			42g[.17]		8.5g[.65]			B. S.	Davies et al.[14]
6.0 MeV	20		40	*4.0(-.6)	*8.8(1.4)		25	B. S.	Davies et al.[13]
8.0 MeV			42g[.35]		25g[.72]			B. S.	Davies et al.[14]
12.0 MeV			67g[.5]		40g[.70]			B. S.	Davies et al.[14]

g:extracted from graph, * used in fits,
( ) indicate fractional standard deviations
[ ] point on Chi-Chi$_0$ graph used to extract dechanneling length

TABLE V

Fits to Hadronic Planar Dechanneling

Crystal & Orientation	Lamda (1/e) (100 GeV, mm)	No. of Points
Si(110)	70.3±10.7	15(all energies)
	74.8±9.0	10(low energy)
	61.3±7.9	5(high energy)
Si(111)	109.4±16.7	9(all energies)
	108.0±17.6	7(low energy)
	114.2	2(high energy)
Ge(110)	60.5±5.9	6(low energy)
W(110)	55.3±2.0	3(low energy)
W(100)	29.8±5.2	3(low energy)

TABLE VI

Positron and Electron Dechanneling Lengths in Silicon

(all lengths are in microns and are 1/e)

Positrons

Energy	Axial <111>	Planar (100)	Planar (110)	Planar (111)	Method	Reference
54		40	60	42	Trans.[a]	Livermore[72]

Electrons

Energy	Axial <111>	Planar (100)	Planar (110)	Planar (111)	Method	Reference
17		16	20(n=1) 17(n=2) 17(n=3)		Trans.[a]	Livermore[72]
54		24	36		Trans.[a]	Livermore[72]
350			31			Komaki et al.[73]
1200	39±4		28±5		Trans.	Adejshvili et al.[74]

a. Livermore errors are estimated to be 25 to 30%

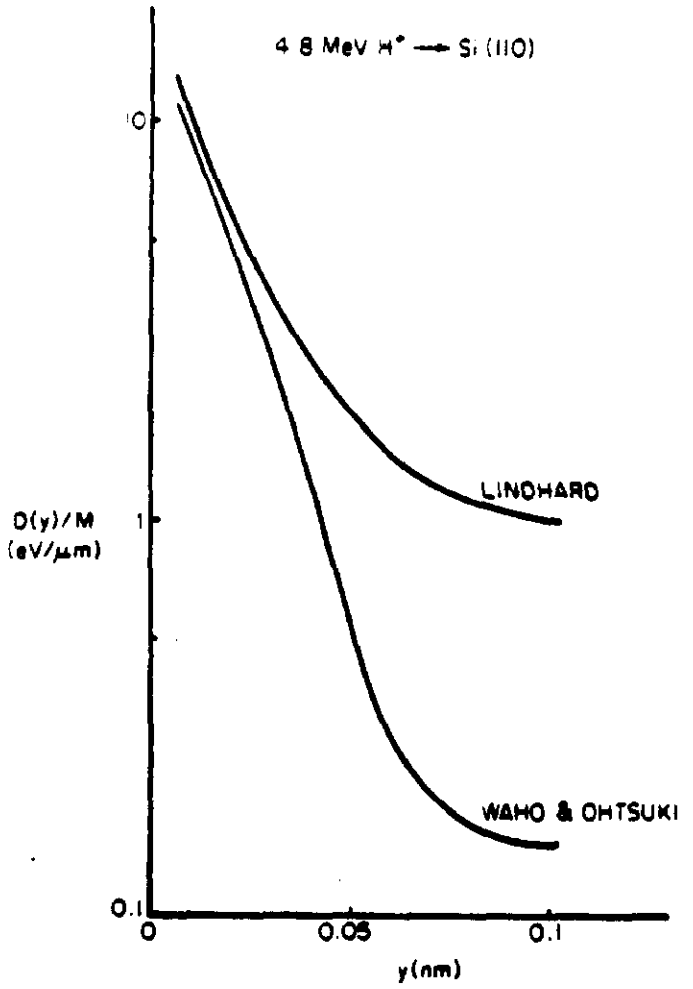
4 8 MeV H⁺ → Si (110)
10
1
0.1
D(y)/M
(eV/μm)
LINDHARD
WAHO & OHTSUKI
0
0.05
0.1
y(nm)

Fig. 1

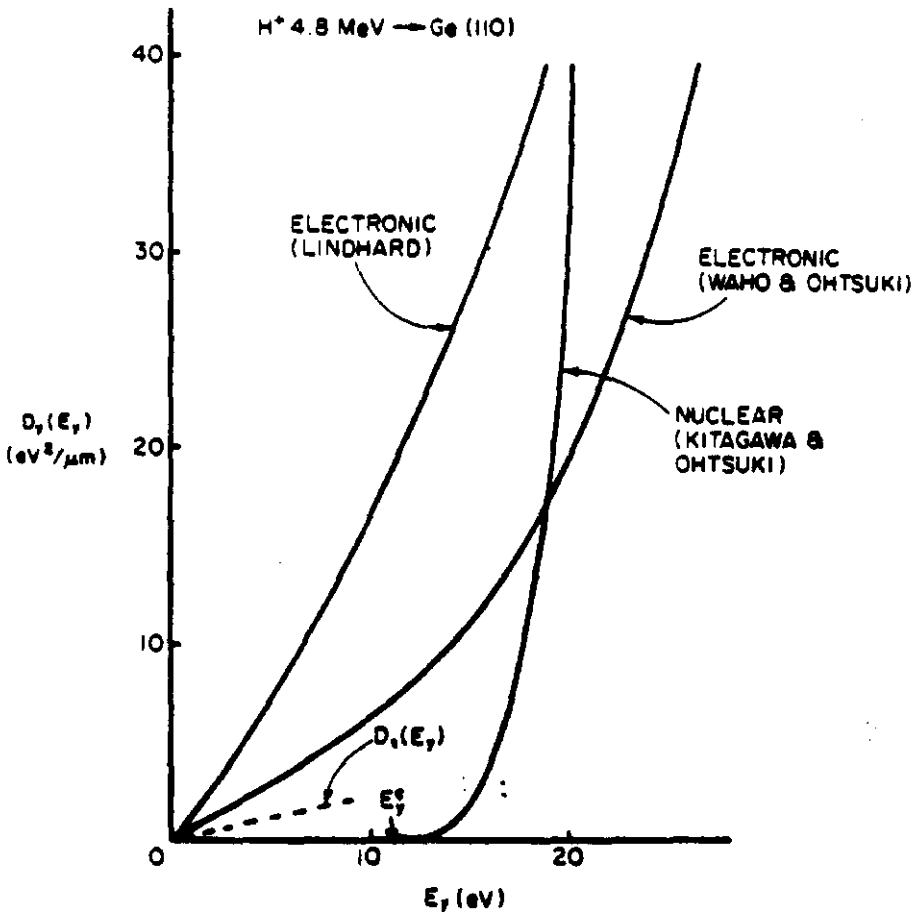
H⁺ 4.8 MeV → Ge (110)
40
30
20
10
0
10
20
$D_y(E_y)$ (eV²/μm)
E_y (eV)
ELECTRONIC (LINDHARD)
ELECTRONIC (WAHO & OHTSUKI)
NUCLEAR (KITAGAWA & OHTSUKI)
$D_y(E_y)$
E_y^c

Fig. 2

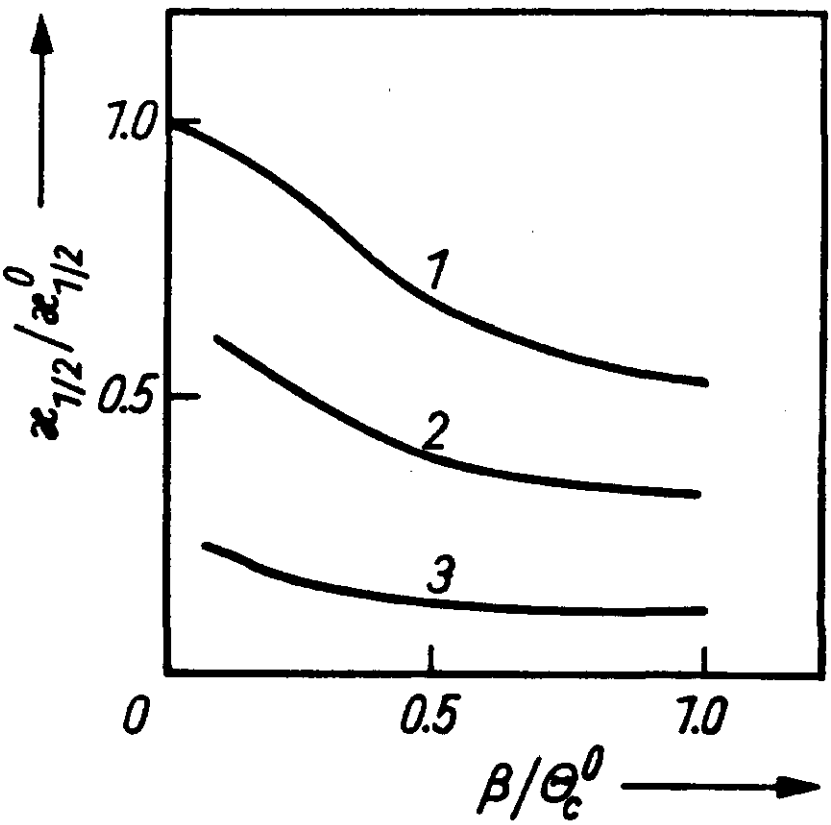

Fig. 3

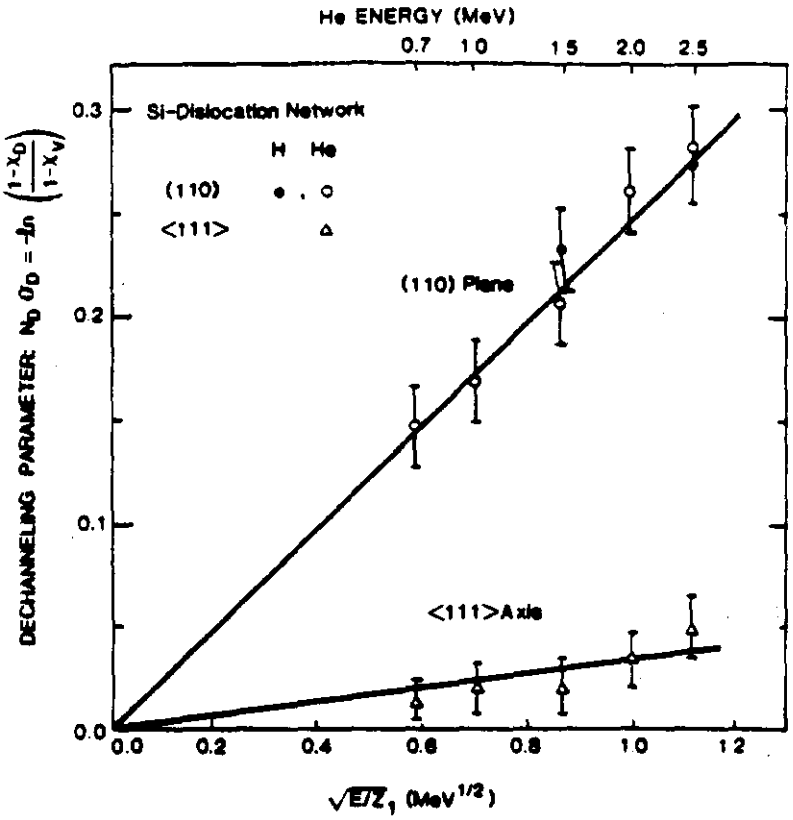
He ENERGY (MeV)
0.7
1.0
1.5
2.0
2.5
Si-Dislocation Network
H He
(110) • , ○
<111> △
(110) Plane
<111>Axis
DECHANNELING PARAMETER $N_D \sigma_D = -\ln\left(\frac{1-\chi_D}{1-\chi_V}\right)$
0.0
0.1
0.2
0.3
0.0
0.2
0.4
0.6
0.8
1.0
1.2
$\sqrt{E/Z_1}$ (MeV$^{1/2}$)

Fig. 4

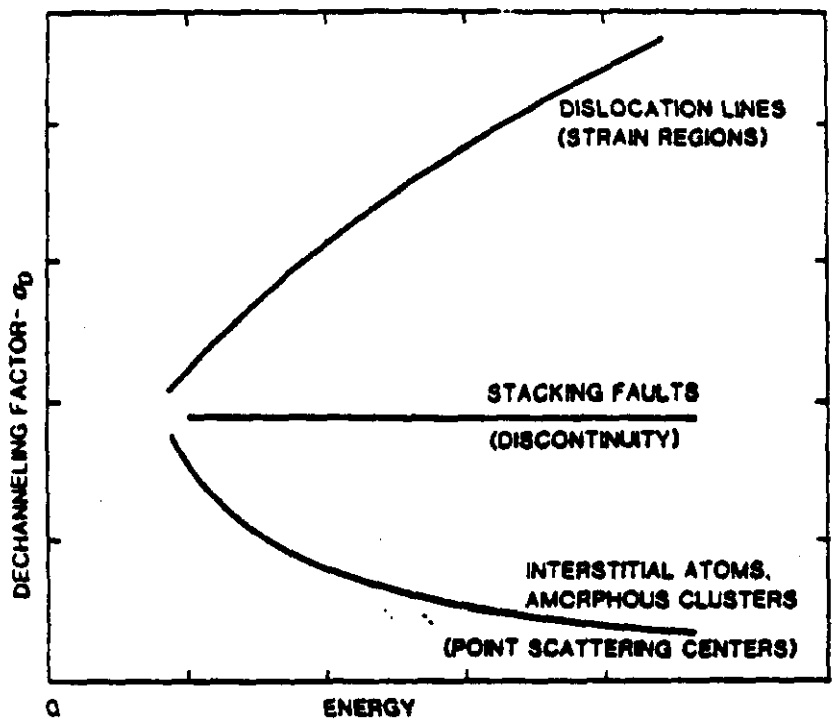
DISLOCATION LINES
(STRAIN REGIONS)
STACKING FAULTS
(DISCONTINUITY)
INTERSTITIAL ATOMS,
AMORPHOUS CLUSTERS
(POINT SCATTERING CENTERS)
DECHANNELING FACTOR- σ_D
0
ENERGY

Fig. 5

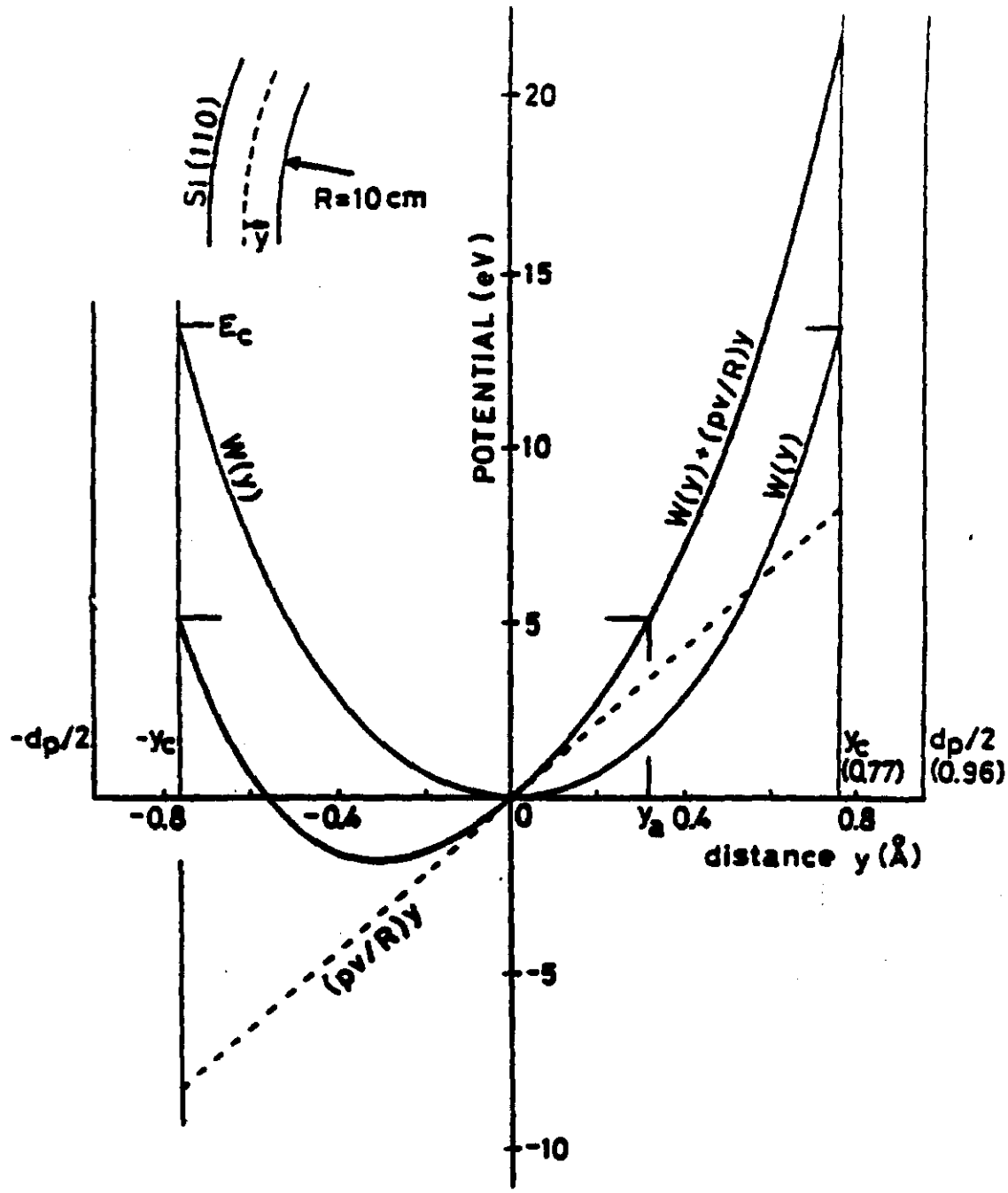
Si(110)
R=10 cm
y
E_c
W(y)
POTENTIAL (eV)
20
15
10
5
-5
-10
W(y)+(pv/R)y
W(y)
$-d_p/2$
$-y_c$
y_c (0.77)
$d_p/2$ (0.96)
-0.8
-0.4
0
y_a 0.4
0.8
distance y (Å)
(pv/R)y

Fig. 6

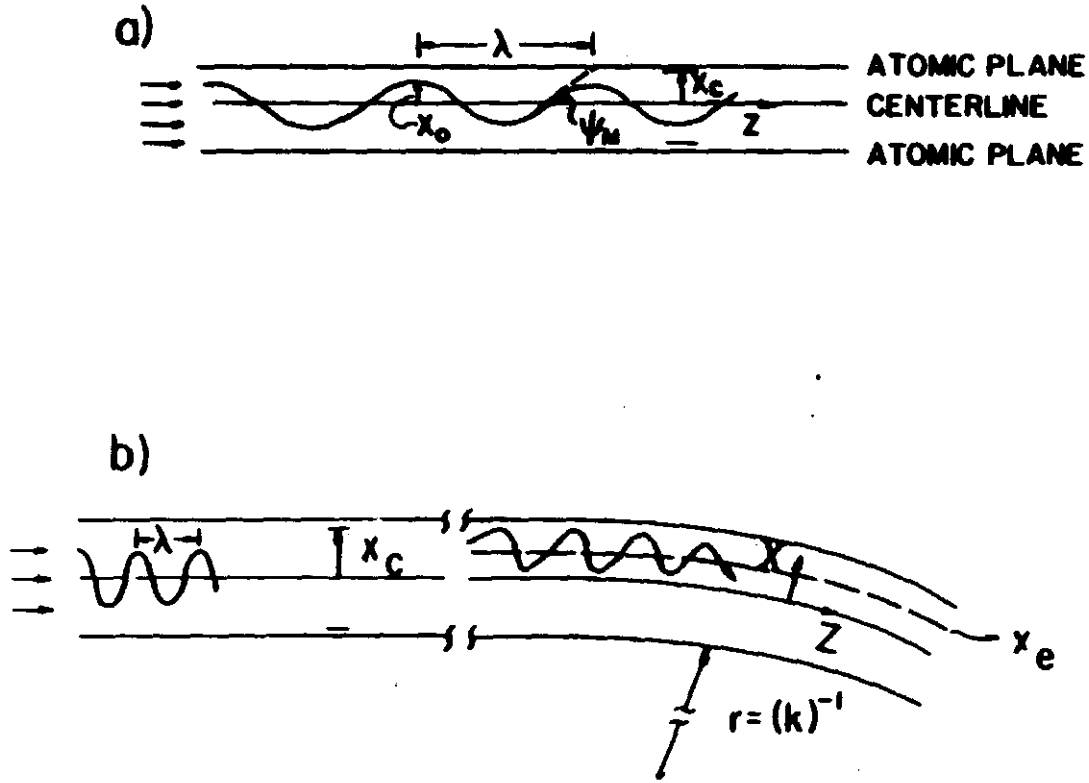
a)
λ
ATOMIC PLANE
CENTERLINE
ATOMIC PLANE
x_c
x_o
ψ_M
z
b)
λ
x_c
x_f
z
x_e
$r=(k)^{-1}$

Fig. 7

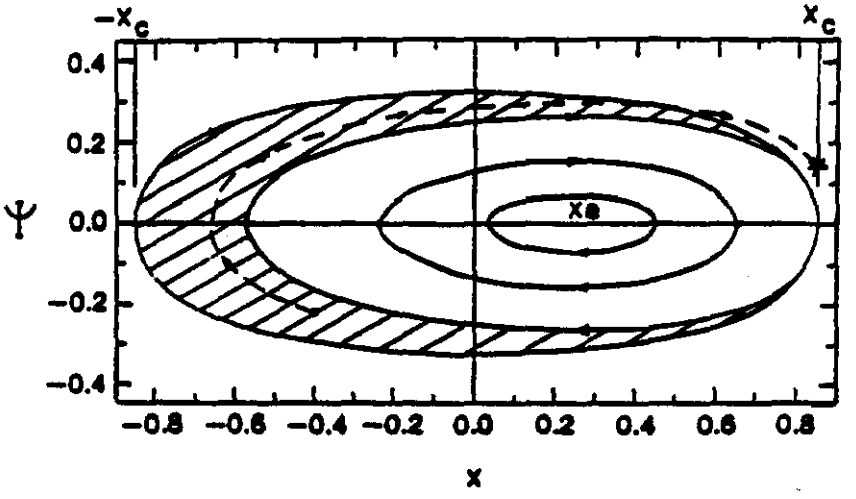

Fig. 8

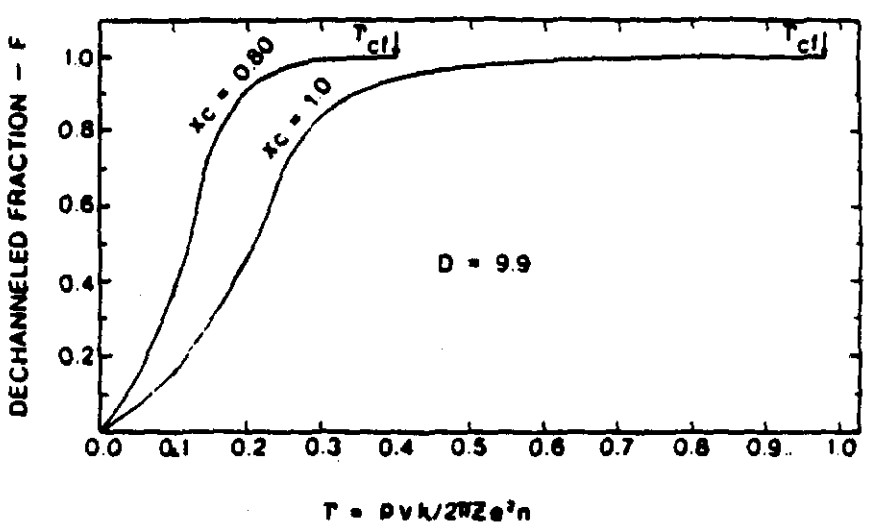
DECHANNELED FRACTION - F
1.0
0.8
0.6
0.4
0.2
0.0
0.1
0.2
0.3
0.4
0.5
0.6
0.7
0.8
0.9
1.0
T_{cl}
T_{cl}
$x_c = 0.80$
$x_c = 1.0$
D = 9.9
T = pvh/2πZe²n

Fig. 9

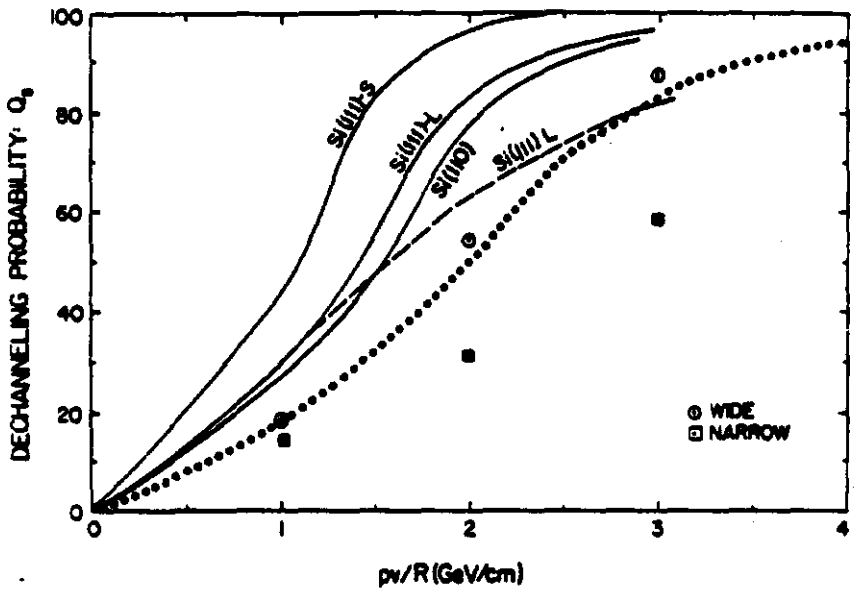
DECHANNELING PROBABILITY, Q_e
pv/R (GeV/cm)
Si(111)-S
Si(111)-L
Si(110)
Si(111) L
WIDE
NARROW
0
20
40
60
80
100
1
2
3
4

Fig. 10

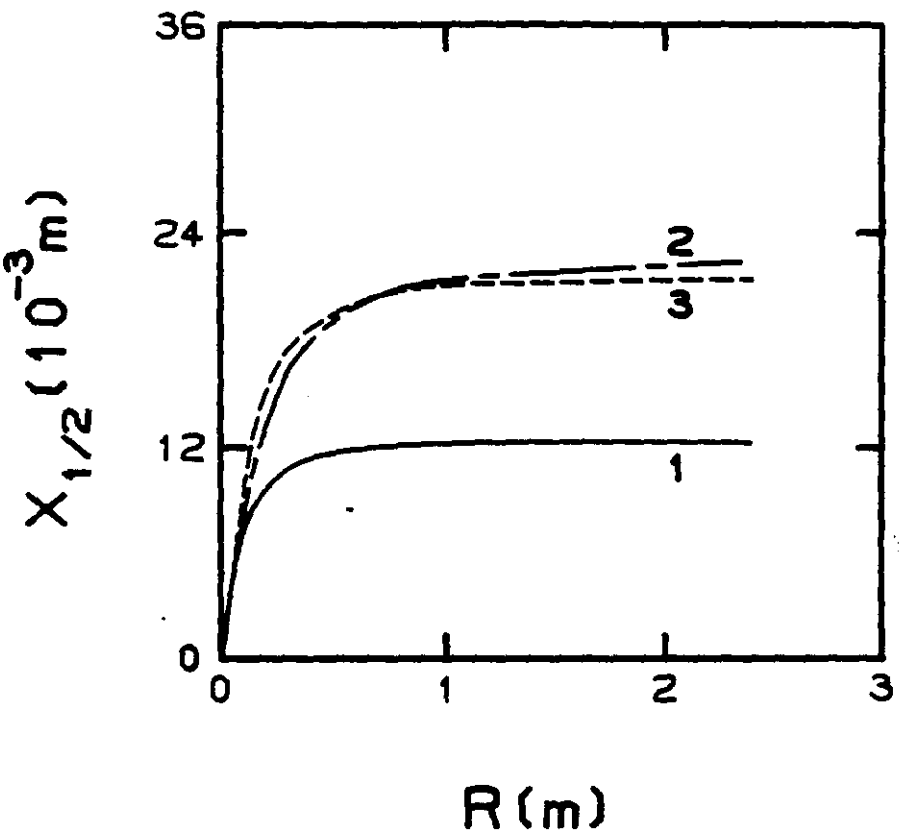

Fig. 11

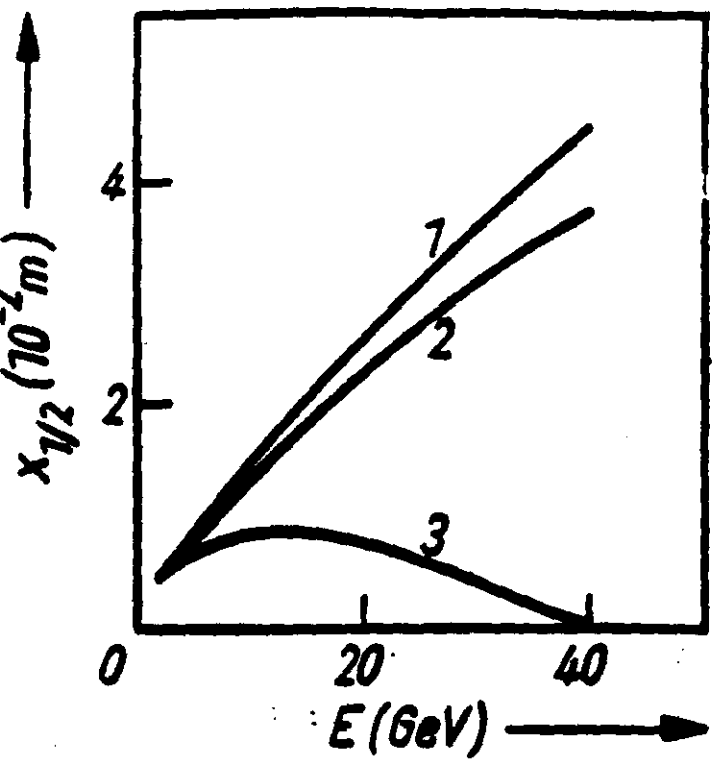

Fig. 12

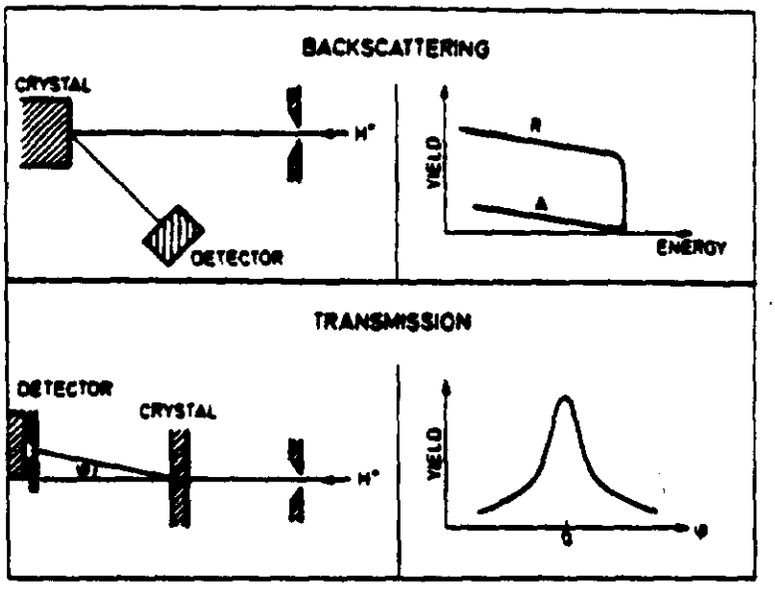
BACKSCATTERING
CRYSTAL
H°
DETECTOR
YIELD
R
A
ENERGY
TRANSMISSION
DETECTOR
CRYSTAL
H°
YIELD
0
ψ

Fig. 13

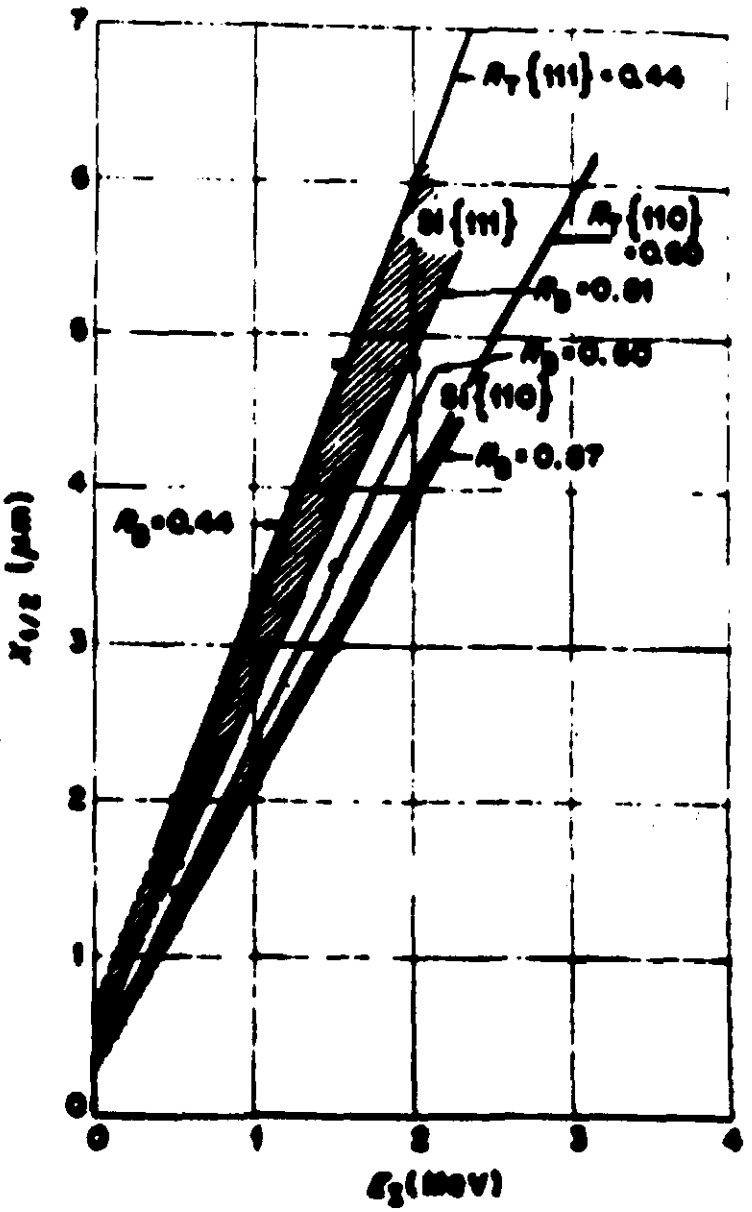

Fig. 14

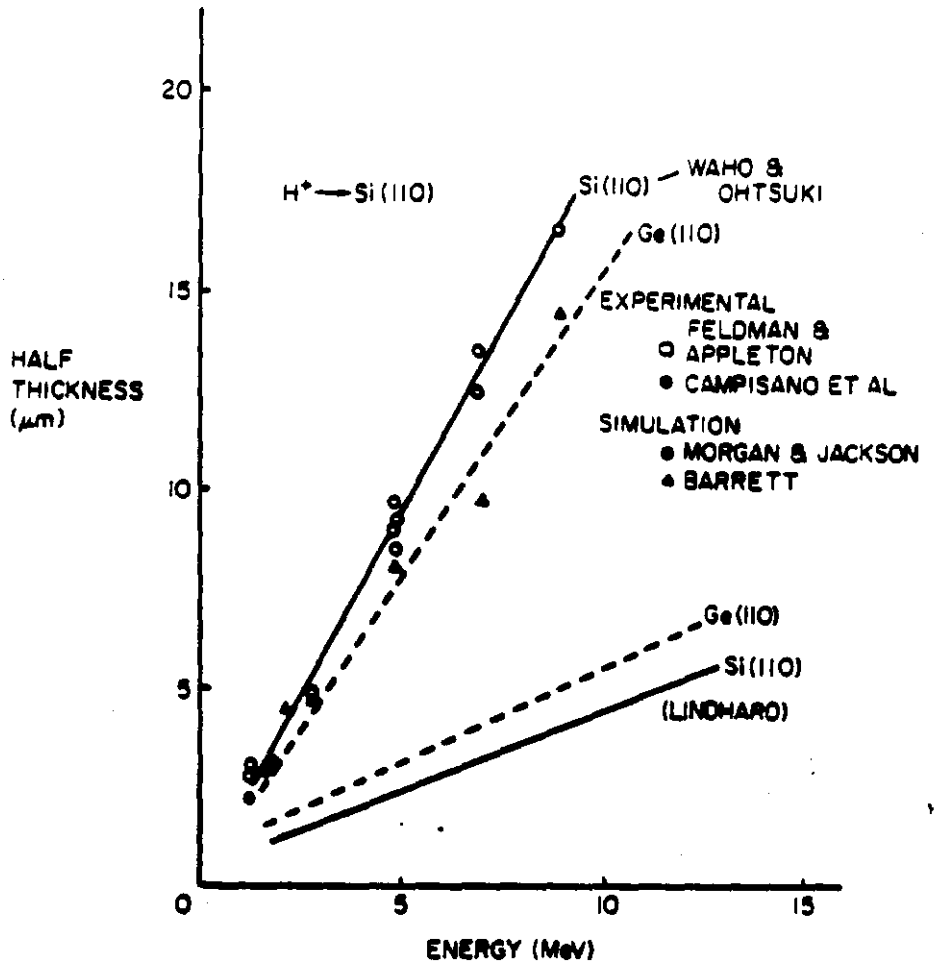
20
15
10
5
0
5
10
15
HALF
THICKNESS
(μm)
ENERGY (MeV)
H⁺—Si (110)
Si (110) — WAHO & OHTSUKI
Ge (110)
EXPERIMENTAL
FELDMAN & APPLETON
CAMPISANO ET AL
SIMULATION
MORGAN & JACKSON
BARRETT
Ge (110)
Si (110)
(LINDHARD)

Fig. 15

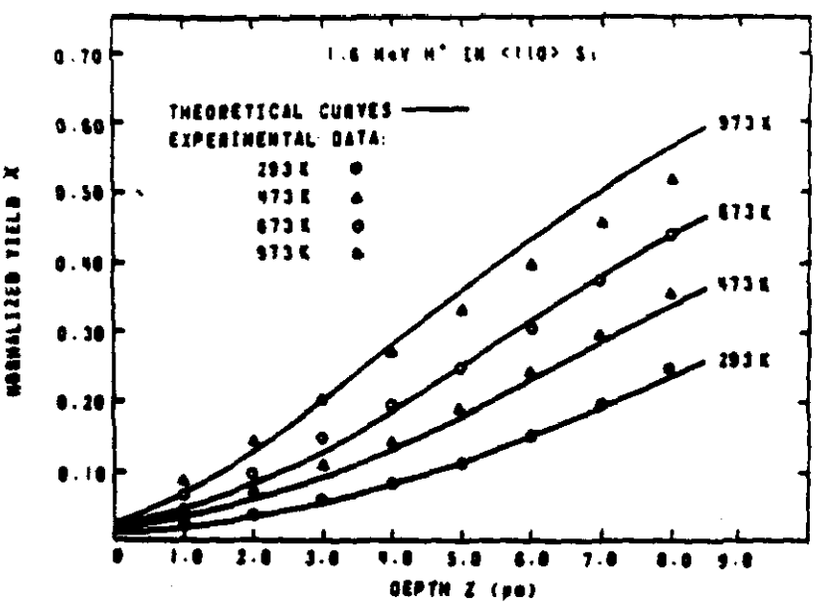
1.6 MeV H⁺ IN <110> Si
THEORETICAL CURVES
EXPERIMENTAL DATA:
293 K
473 K
673 K
973 K
NORMALIZED YIELD χ
DEPTH Z (μm)
0.70
0.60
0.50
0.40
0.30
0.20
0.10
0
1.0
2.0
3.0
4.0
5.0
6.0
7.0
8.0
9.0

Fig. 16

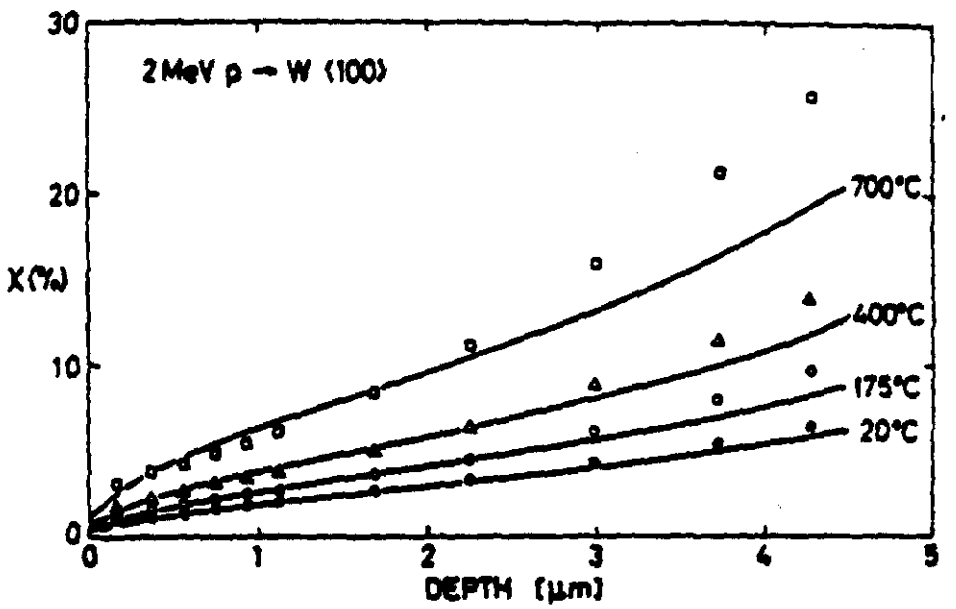

Fig. 17

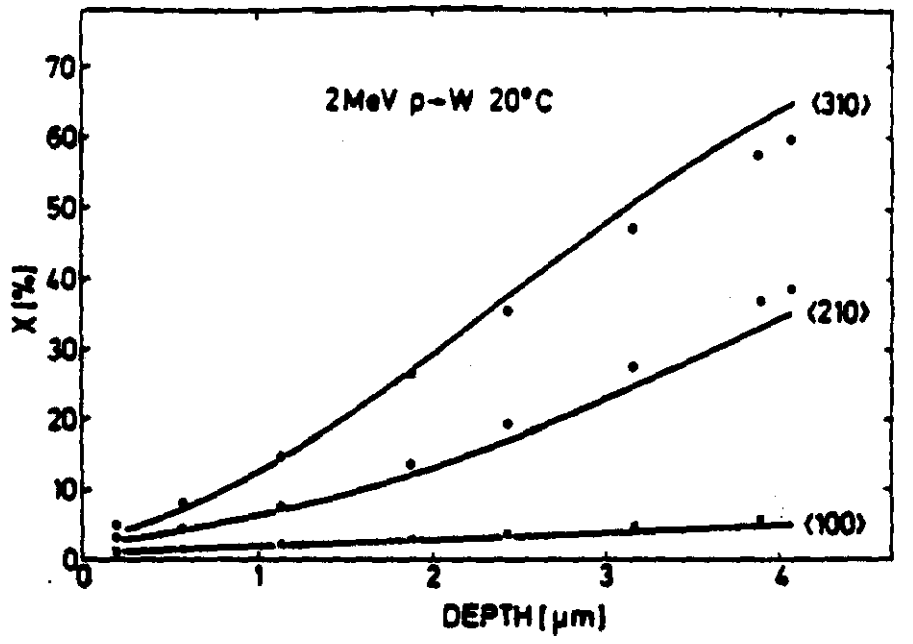

Fig. 18

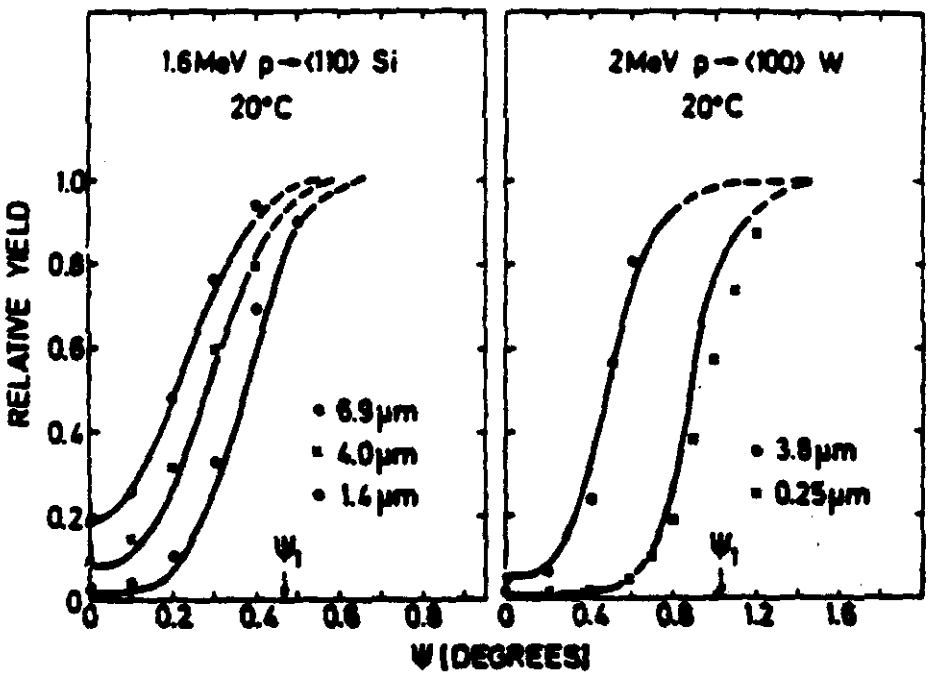
1.6MeV p→⟨110⟩ Si
20°C
2MeV p→⟨100⟩ W
20°C
RELATIVE YIELD
1.0
0.8
0.6
0.4
0.2
0
• 6.9μm
▪ 4.0μm
• 1.4μm
• 3.8μm
▪ 0.25μm
Ψ_1
0
0.2
0.4
0.6
0.8
0
0.4
0.8
1.2
1.6
Ψ (DEGREES)

Fig. 19

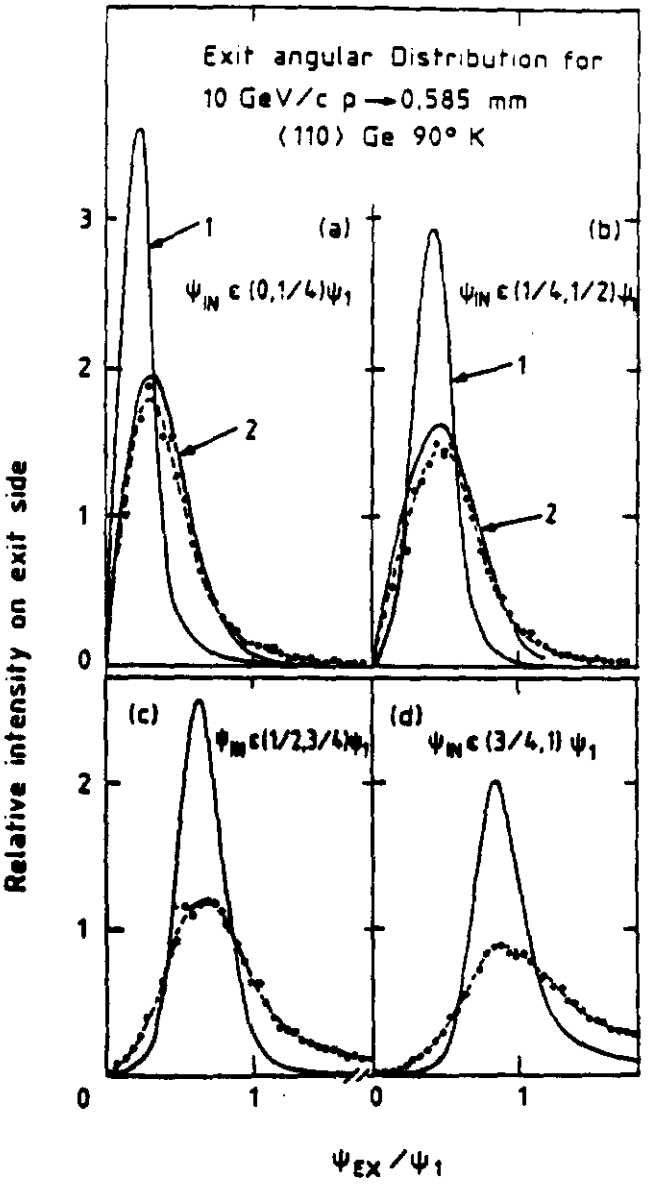
Exit angular Distribution for
10 GeV/c p → 0.585 mm
⟨110⟩ Ge 90° K
(a)
(b)
(c)
(d)
1
2
$\psi_{IN} \in (0,1/4)\psi_1$
$\psi_{IN} \in (1/4,1/2)\psi_1$
$\psi_{IN} \in (1/2,3/4)\psi_1$
$\psi_{IN} \in (3/4,1)\psi_1$
Relative intensity on exit side
ψ_{EX}/ψ_1
0
1
2
3

Fig. 20

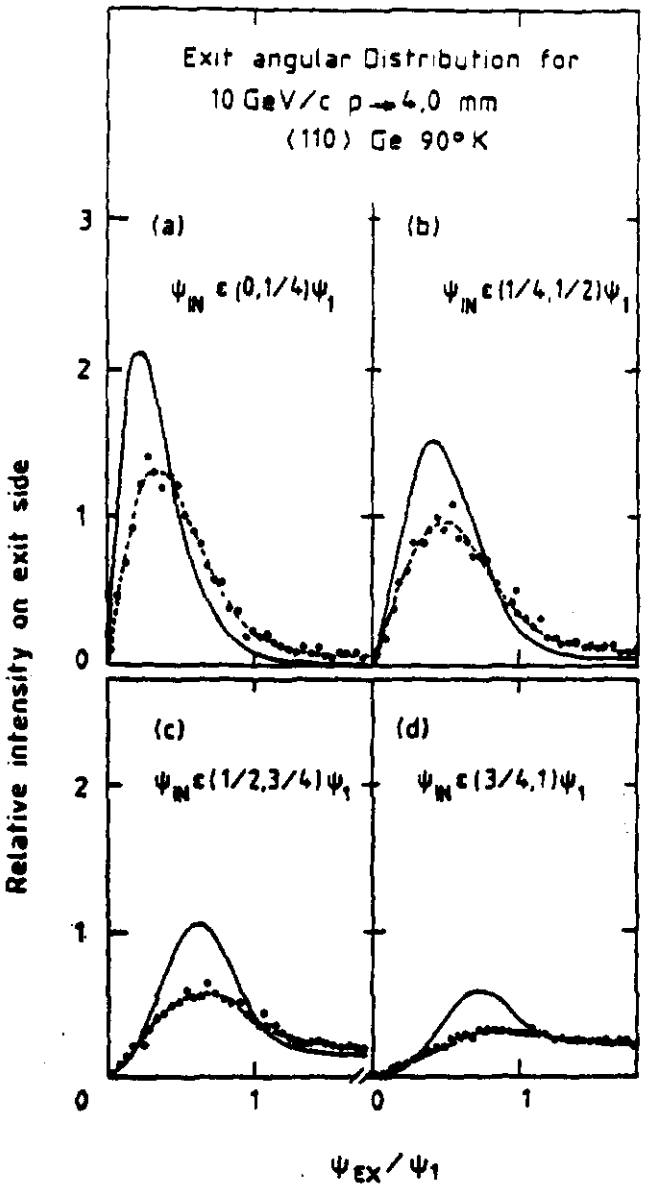
Exit angular Distribution for
10 GeV/c p → 4.0 mm
(110) Ge 90° K
(a)
ψ_{IN} ε (0,1/4)ψ_1
(b)
ψ_{IN} ε (1/4,1/2)ψ_1
(c)
ψ_{IN} ε (1/2,3/4)ψ_1
(d)
ψ_{IN} ε (3/4,1)ψ_1
Relative intensity on exit side
ψ_{EX}/ψ_1

Fig. 21

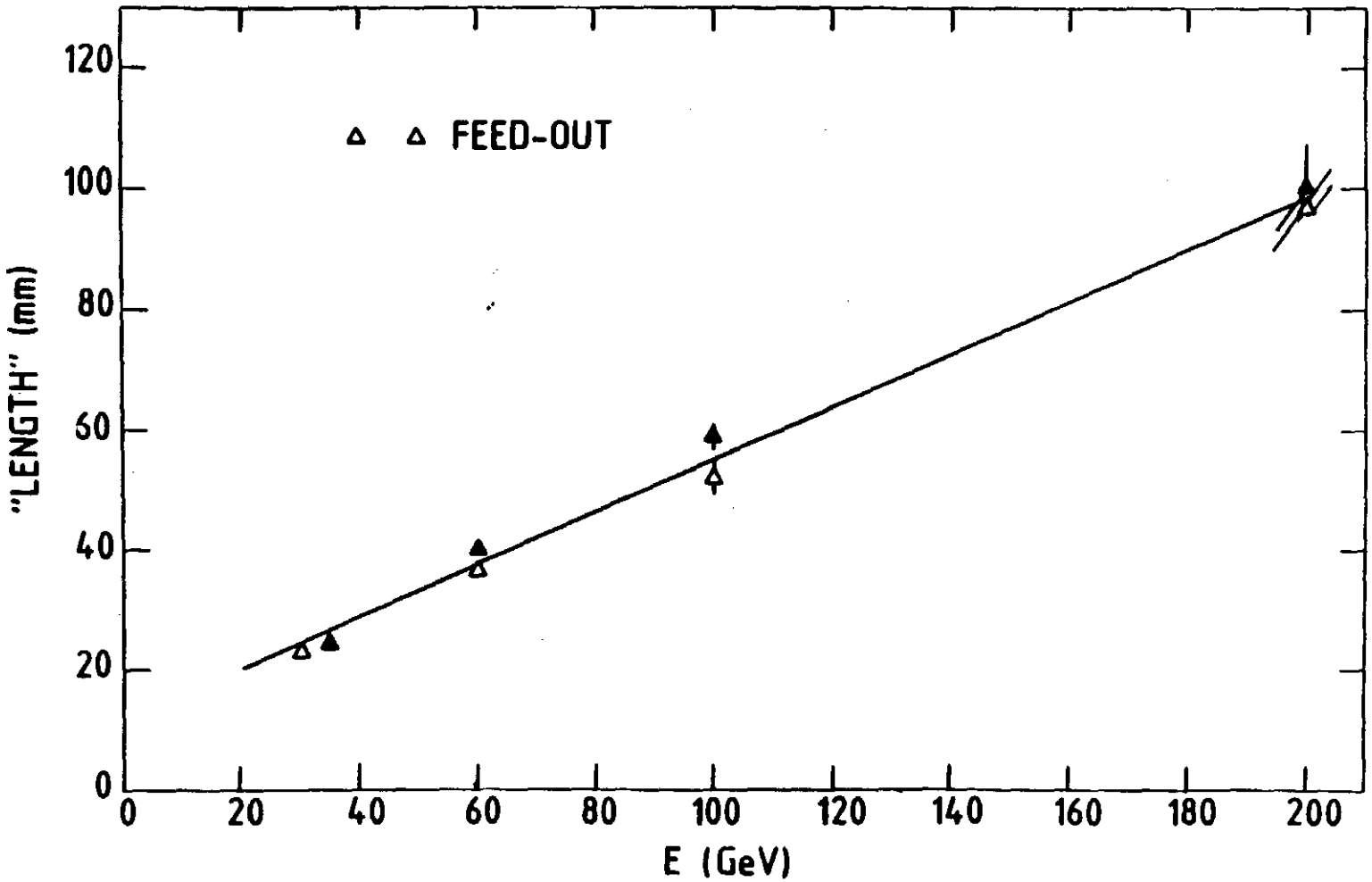

Fig. 22

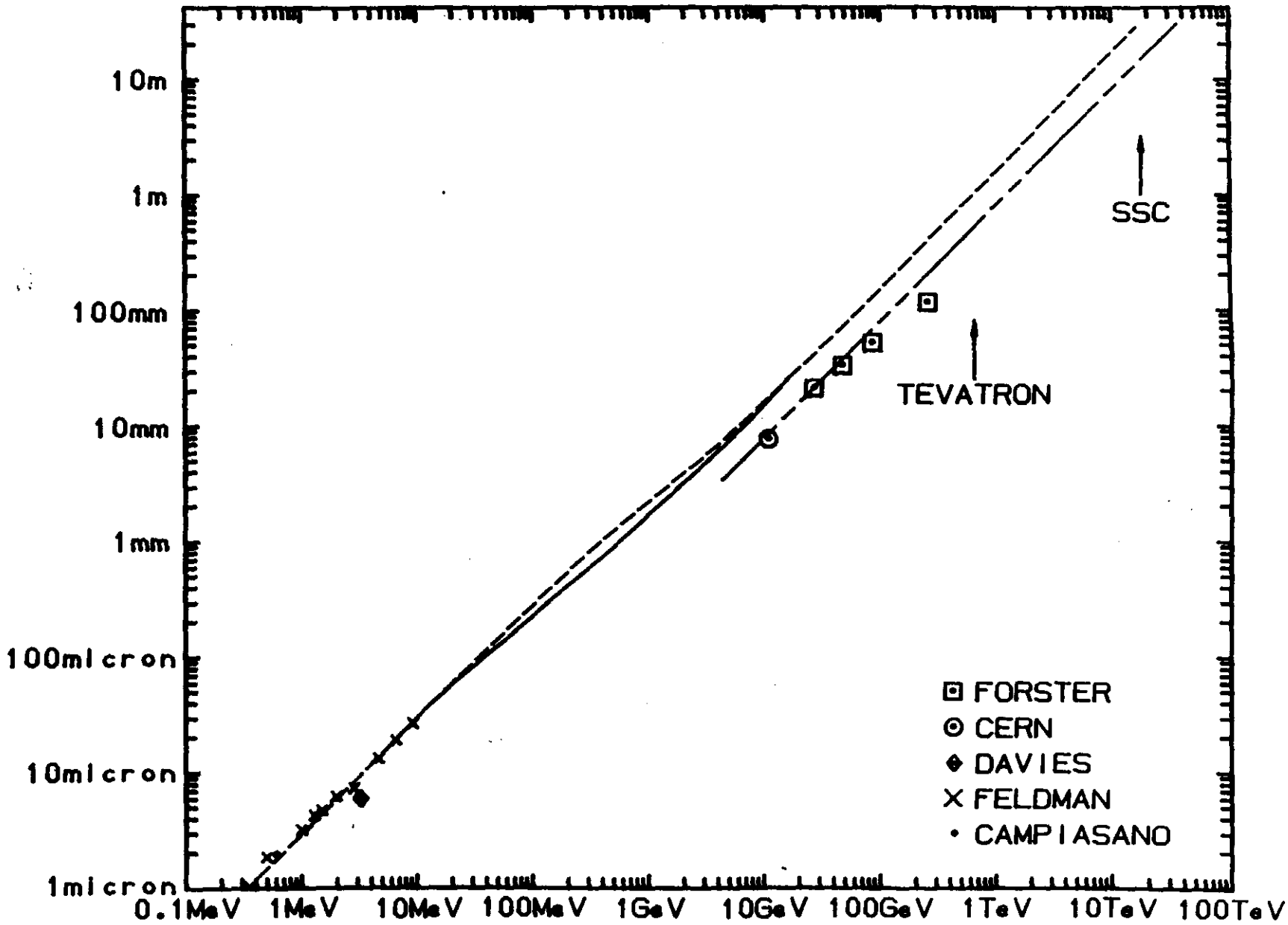
10m
1m
100mm
10mm
1mm
100micron
10micron
1micron
0.1MeV
1MeV
10MeV
100MeV
1GeV
10GeV
100GeV
1TeV
10TeV
100TeV
SSC
TEVATRON
FORSTER
CERN
DAVIES
FELDMAN
CAMPIASANO

Fig. 23

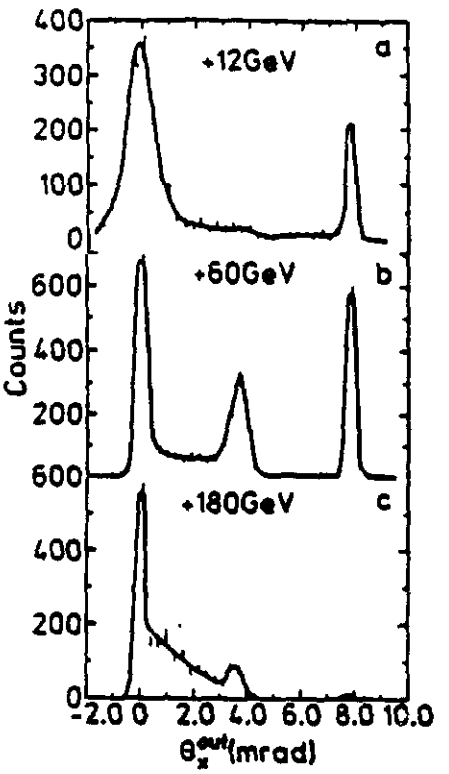
400
300
200
100
0
+12GeV
a
600
400
200
600
400
200
+60GeV
b
Counts
600
400
200
0
+180GeV
c
-2.0 0 2.0 4.0 6.0 8.0 10.0
θ_x^{out}(mrad)

Fig. 24

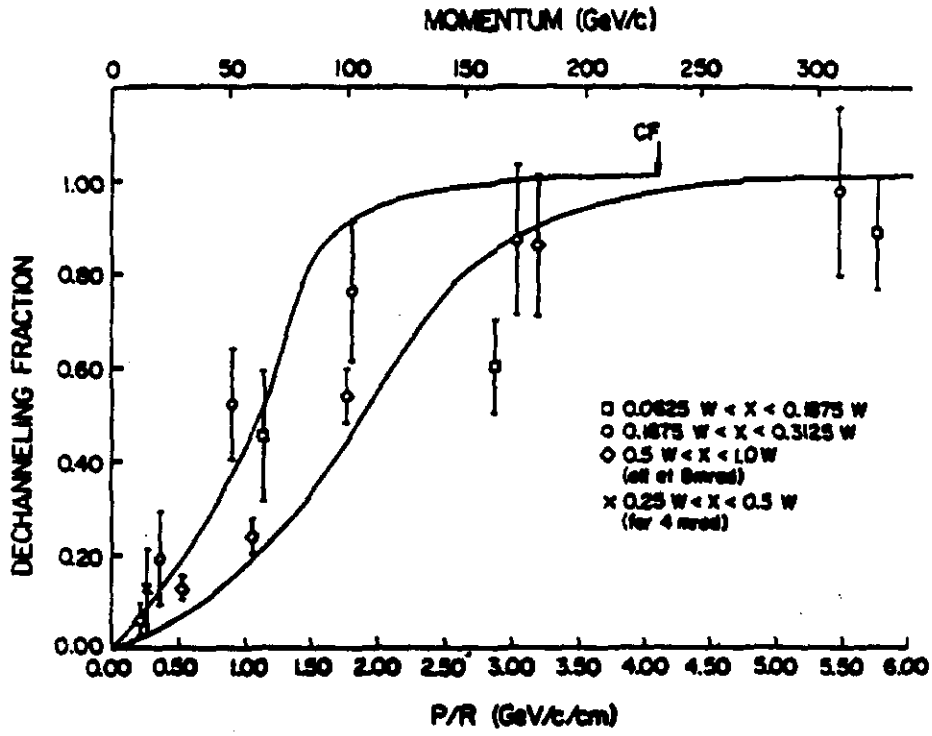
MOMENTUM (GeV/c)
0
50
100
150
200
250
300
CF
1.00
0.80
0.60
0.40
0.20
0.00
DECHANNELING FRACTION
0.00
0.50
1.00
1.50
2.00
2.50
3.00
3.50
4.00
4.50
5.00
5.50
6.00
P/R (GeV/c/cm)
0.0625 W < X < 0.1875 W
0.1875 W < X < 0.3125 W
0.5 W < X < 1.0 W
(all at 8mrad)
0.25 W < X < 0.5 W
(for 4 mrad)

Fig. 25

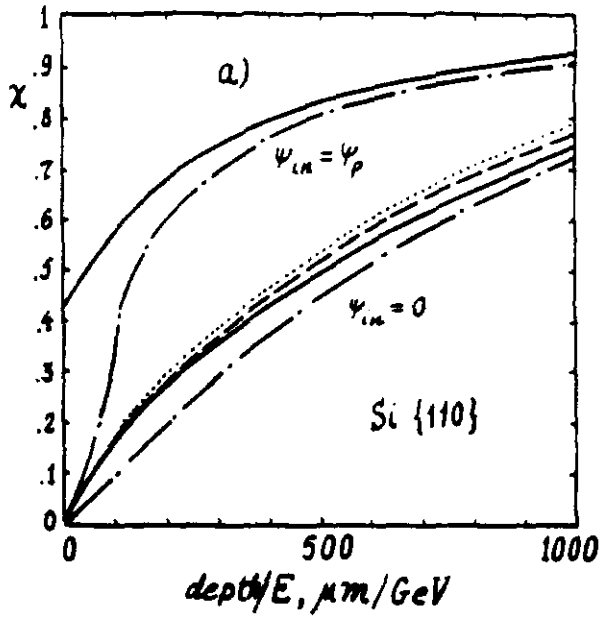
a)
χ
$\psi_{in} = \psi_p$
$\psi_{in} = 0$
Si {110}
0
500
1000
depth/E, μm/GeV

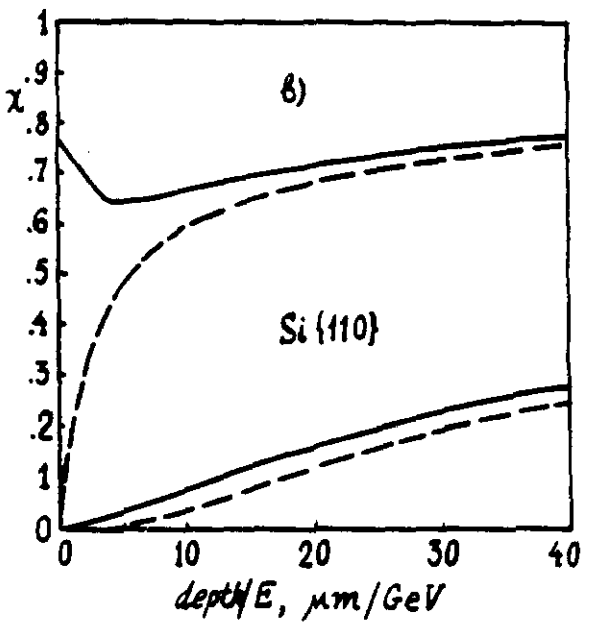
б)
χ
Si {110}
0
10
20
30
40
depth/E, μm/GeV

Fig. 26